PAPER TITLE:

Multi-scale analysis of settlement-induced building damage using damage surveys and DInSAR data: a case study in The Netherlands

Authors: Dario Peduto[a*], Gianfranco Nicodemo[a], Jos Maccabiani[b], Settimio Ferlisi[a]

[a] Department of Civil Engineering
University of Salerno
Via Giovanni Paolo II, 132
84084 - Fisciano (SA
e-mail: dpeduto@unisa.it; gnicodemo@unisa.it; sferlisi@unisa.it.

[b] work carried out while at SkyGeo Netherlands B.V.
current correspondence address:
Science and Technology Corporation BV,
Olaf Palmestraat 14, 2616 LR Delft,
The Netherlands
e-mail: jos.maccabiani@stcorp.nl

Corresponding author:

[*]Dario Peduto
Department of Civil Engineering
University of Salerno
Via Giovanni Paolo II, 132
84084 - Fisciano (SA)
e-mail: dpeduto@unisa.it
Tel. +39 089 964120; Mobile +39 3286935656

This is a post-peer-review, pre-copyedit version of an article published in **ENGINEERING GEOLOGY**.

The final authenticated version is available online at: **http://dx.doi.org/10.1016/j.enggeo.2016.12.018**

This is a post-peer-review, pre-copyedit version of an article published in **ENGINEERING GEOLOGY**. The final authenticated version is available online at: **http://dx.doi.org/10.1016/j.enggeo.2016.12.018**

Abstract

Highly compressible clayey and peaty (soft) soils may expose structures (e.g. buildings) and infrastructures (e.g. roads and embankments) resting on them to absolute/differential settlements. These latter, with passing of time, can induce damages whose level of severity depends on several factors such as: the spatial distribution of the thickness pertaining to soft soil layers; the groundwater regime; the characteristics of the exposed structures and infrastructures along with their state of maintenance. The analysis of damages and the resulting management of the built-up environment usually require high costs due to both the amount of data necessary for setting up reliable forecasting models as well as for defining the most suitable restoration works. This paper presents a multi-scale procedure tailored to analyse the settlement-induced building damage. The selected case study deals with an urban area in The Netherlands where, at medium scale, the role of soft soils in predisposing the occurrence of ground surface settlements is first investigated. Then, at large scale the relationship between cause (i.e. settlements) and effects (i.e. damage) is analysed for building aggregates via the combination of high-resolution advanced differential interferometric synthetic aperture radar (DInSAR) and in-situ damage survey data. Finally, as main novelty of the proposed multi-scale procedure, both the above datasets are used to generate, at detailed scale, empirical fragility curves for single buildings that, once further validated, could be valuably adopted for damage forecasting purposes in similar urban areas.

Keywords: Settlements; building damage; DInSAR; shallow/piled foundations, soft soils, fragility curves.

1. Introduction

Many parts of the world are affected by ground subsidence. This originates either from natural processes such as physical and chemical soil weathering or from anthropogenic activities such as groundwater withdrawals, mining and tunneling construction (Holzer, 2009). Independently of the nature of the triggering factors, the magnitude and rate of the displacement patterns experienced by the subsoil can be strongly conditioned by the presence and continuity of layers of fine-grained "soft soils" containing (organic) clays and peat. These types of soils are characterized by a very high compressibility in both primary and secondary (or creeping) consolidation stages (Den Haan and Kruse, 2006). The compressibility might be further amplified by changes in the ionic content of the pore water (Cascini and Di Maio, 1994; Huat, 2004).

As a result, structures (e.g. buildings) and infrastructure networks (e.g. pipelines, roads and embankments) in subsiding geological environments may suffer from absolute and/or differential settlements causing damages of various levels of severity. This is testified by a number of case histories that show economic losses of billions of dollars per year (Buex et al., 2015). For this reason, the analysis of damages to (infra)structures at subsidence risk is a topic of particular concern for both scientific and technical communities when the most suitable strategies for land-use planning and urban management have to be identified.

Carrying out this analysis is a difficult task. It requires a deep knowledge on the characteristics of the exposed (infra)structures as well as stratigraphy, physical/mechanical properties and groundwater regime of soft soil deposits. Furthermore, gathering information on the spatial distribution and severity of damages suffered by (infra)structures, along with the associated settlement rates they experienced during the damage process, is essential for developing reliable forecasting models. As for settlement rates, the latest generation of

This is a post-peer-review, pre-copyedit version of an article published in **ENGINEERING GEOLOGY**. The final authenticated version is available online at: **http://dx.doi.org/10.1016/j.enggeo.2016.12.018**

spaceborne synthetic aperture radar (SAR) sensors currently provides scientists and technicians with huge datasets of very high resolution images that, processed via advanced differential interferometric techniques (DInSAR), allow detecting and mapping the settlements (over a given period of time) that pertain to points either on the ground surface or on the exposed (infra)structures. The combination of the DInSAR-derived settlements with the recorded damages (such as cracks on building façades and deformations of road pavements) can provide a cognitive basis helpful to establish empirical cause-effect relationships that, once validated, can be later adopted to develop damage forecasting models.

This paper presents a multi-scale procedure specifically oriented to the analysis of settlement-induced damage to buildings resting on shallow/piled foundations on soft soils. The proposed procedure – which benefits from information concerning the characteristics of the local subsoil, the DInSAR-derived settlements of the buildings and the damage recorded to these buildings via field surveys – is applied to densely urbanized areas in the south-western part of The Netherlands where the shallow subsoil mainly consists of about 20 meters of alternating clayey and peaty soil layers.

2. Damage assessment

Building damageability criteria well-adopted in geotechnical engineering practice (Bjerrum, 1963; Boscardin and Cording, 1989; Burland and Wroth, 1974; Polshin and Tokar, 1957; Skempton and MacDonald, 1956) show that the damage severity on superstructures depends on the magnitude of the subsidence-related intensity (SRI) parameters experienced by the foundation system. SRI parameters are e.g. settlements, differential settlements, angular distortions and relative rotations. Moreover, the damage severity on superstructures may vary according to *i)* the year and technique of construction, *ii)* the state of maintenance and *iii)* the

This is a post-peer-review, pre-copyedit version of an article published in **ENGINEERING GEOLOGY**. The final authenticated version is available online at: **http://dx.doi.org/10.1016/j.enggeo.2016.12.018**

characteristics (such as geometry, number of floors, materials and foundation typology) of buildings at subsidence risk. These criteria can be categorized in two main classes. In particular, the "analytical" criteria are based on the adoption of mathematical relationships between SRI parameter values and damage severity to superstructures when they are modeled, for instance, to behave as an elastic beam (Boscardin and Cording, 1989; Burland and Wroth, 1974). On the other hand, the "empirical" criteria consist of relationships between the SRI parameter values and the damage severity, in turn relatable to the crack patterns – recorded by in-situ surveys – which may affect either non-structural (i.e. infill walls, panels) or structural (i.e. pillars, beams) building elements (Burland et al., 1977; Burland and Wroth, 1974; Cooper, 2008). It is worth observing that the above relationships, for both classes of damageability criteria, can deal with a "single building" or a "set of buildings" depending on the scale of work (Cascini et al., 2013a; Peduto et al., 2016c; van Westen et al., 2008). Moreover, they can be expressed in terms of "fragility curves" which provide, usually on the basis of log-normal functions, the conditional probability for a single building or a set of buildings to be in, or exceed, a certain damage state under a phenomenon (or danger) of given intensity (Mavrouli et al., 2014; Negulescu et al., 2010; Peduto et al., 2016b, 2016c; Saeidi et al., 2012). These curves, once properly validated, could turn out to be a useful tool to predict the level of damage severity to buildings at subsidence risk.

3. DInSAR techniques

Images acquired by spaceborne Synthetic Aperture Radar (SAR) sensors and processed via advanced differential Interferometric techniques (DInSAR) represent a well-established tool for analyzing the effects induced by many natural or anthropogenic phenomena in different fields – among which earthquakes (Prati et al., 2010; Reale et al., 2011), volcanology

This is a post-peer-review, pre-copyedit version of an article published in **ENGINEERING GEOLOGY**. The final authenticated version is available online at: **http://dx.doi.org/10.1016/j.enggeo.2016.12.018**

(Catalano et al., 2014; Lee et al., 2013), slow-moving landslides (Bianchini et al., 2013; Calò et al., 2012, 2014; Cascini et al., 2013a; Gullà et al., 2016; Herrera et al., 2013; Peduto et al., 2016c; Tofani et al., 2014; Wasowski and Bovenga, 2014), mining (Carnec et al., 1995; Crosetto et al., 2005; Herrera et al., 2010; Raucoles et al., 2003), water extraction (Cascini et al., 2006; Cigna et al., 2012; Herrera et al., 2009b; Peduto et al., 2015; Sanabria et al., 2014; Tomás et al., 2014), underground construction works (Bandini et al., 2015; Giannico et al., 2012) as well as for monitoring of (infra)structures (Arangio et al., 2013; Cascini et al., 2013b; Costantini et al., 2014; Nicodemo et al., 2016; Peduto et al., 2015, 2016a; Perissin et al., 2009; Pratesi et al., 2015b; Tomás et al., 2013) and for addressing multi-risk issues (Pazzi et al., 2016).

The available techniques for the analysis of phase signals in interferometric stacks can be grouped in two main classes: Persistent Scatterers Interferometry (PSI) (Costantini et al., 2008; Crosetto et al., 2008; Ferretti et al., 2000, 2001) and Small-Baseline (SBAS) approaches (Berardino et al., 2002; Fornaro et al., 2009). PSI techniques operate at full spatial resolution and identify reliable scatterers by measuring their multitemporal coherence related to the phase stability; monitored scatterers (i.e. persistent scatterers, PS) correspond to man-made structures (buildings, roads, bridges) or bare rocks whose size is smaller compared to the system resolution. Conversely, the SBAS techniques are tailored to detect scatterers that may be distributed in the resolution cell or characterized by slow temporal change of scattering properties and to measure ground deformations over large areas (Berardino et al., 2002; Peduto et al., 2015). In these techniques the interferograms are generated according to small temporal and spatial separation constraints in order to further reduce decorrelation effects associated with possible coherence losses typically present in the analysis of rural areas.

This is a post-peer-review, pre-copyedit version of an article published in **ENGINEERING GEOLOGY**. The final authenticated version is available online at: **http://dx.doi.org/10.1016/j.enggeo.2016.12.018**

More recently, algorithms have been developed to apply the same technique to both traditional point targets, i.e. targets captured by a single pixel that contains one dominant scatterer, as well as extended targets, i.e. targets that spread over a collection of pixels, each of which contains multiple nondominant scatterers, usually referred to as distributed scatterers (DS). Examples of DS are homogeneous ground patches in deserts and in non-cultivated lands (Fornaro et al., 2014a; Fornaro et al., 2015). The PS-derived velocity is acquired along the radar line of sight (LOS) with reference to a fixed point on the ground (reference point) and with a sub-millimeter accuracy on the average velocity and sub-centimeter accuracy on the single displacement measure (Hanssen, 2003; Herrera et al., 2009a). An experimental evidence of the possibility to achieve an accuracy up to the order of 1 mm on a single displacement measurement is provided by Fornaro et al. (2013). Each PS is associated with a coherence value, ranging from 0 up to 1, which indicates how the measurement fits the model assumed for the displacement. Recently, the monitoring of ground displacements in built-up urban areas at detailed scale has been significantly enhanced by the last generation X-band high resolution SAR sensor TerraSAR-X/TanDEM-X (TSX/TDX) mission of the GermanAerospace Center (DLR) and the COSMO-SkyMed (CSK) constellation of the Italian Space Agency (ASI) (Cascini et al., 2013b; Fornaro et al., 2014b; Herrera et al., 2010; Peduto et al., 2015, 2016a, 2016b). The resolution improvement allows more details of single facilities to be observed and hence their precise monitoring (Fornaro et al., 2012, 2013; Gernhardt et al., 2010; Nicodemo et al., 2016; Reale et al., 2011; Zhu and Bamler, 2010).

4. Methodology

The proposed methodology is aimed at analyzing settlement-induced damages to buildings whose foundations rest on compressible subsoil (Fig. 1).

This is a post-peer-review, pre-copyedit version of an article published in **ENGINEERING GEOLOGY**. The final authenticated version is available online at: **http://dx.doi.org/10.1016/j.enggeo.2016.12.018**

Following three cascading steps, different goals can be pursued starting from a set of input data including: *i)* geo-lithological properties of the involved soils; *ii)* spaceborne PSI-derived displacement measurements; *iii)* fact-sheets collecting information gathered from the visual inspection of crack patterns experienced by buildings via in-situ damage surveys and *iv)* building characteristics such as the structural typology and foundation type, the number of floors and the state of maintenance.

The first step (Phase 0) of the methodology is carried out at medium scale over large areas for the identification of factors predisposing to ground displacements (see also Sanabria et al., 2014). It consists of the comparison of the cumulative thickness of soft soils with the "free-field" cumulative settlements recorded from PSI data. To this aim, PSI data are preliminarily separated, based on their elevation, in PS at ground level and PS on (top of) the buildings, see §5.2 of this paper. Then, "free field" cumulative settlements (i.e. derived from PS at ground level) are computed by multiplying the PS average velocities along the vertical direction for the acquisition period of SAR images. The separation in height is necessary because more often than not, buildings are founded on piles reaching stable soils and the PS data from those buildings are not representative of the factors predisposing to ground displacements.

Phase 1, carried out at large scale, includes different steps in order to detect the elements at subsidence risk – in terms of building aggregates (Cascini et al., 2013a; Peduto et al., 2016c) – and, subsequently, analyze their settlements. In particular, after fixing a movement threshold on PSI velocity, different possible scenarios for building aggregates and areas surrounding the buildings are identified by comparing the velocities exhibited by PS at ground level and on (top of) the buildings. This allows distinguishing possible ground displacements and related effects on either buildings or infrastructures and utilities (e.g. roads, sidewalks, sewers, pipelines, etc.) or both of them. Then, PSI data on (top of) the buildings

This is a post-peer-review, pre-copyedit version of an article published in **ENGINEERING GEOLOGY**. The final authenticated version is available online at: **http://dx.doi.org/10.1016/j.enggeo.2016.12.018**

allow the computation of settlements and settlement gradients (Cascini et al., 2006, 2007, 2013b; Peduto et al., 2015) suffered by building aggregates. Finally, referring to settlement profiles along the longitudinal cross-section, the maximum values of settlement gradients recorded by each building aggregate are associated with the average level of damage severity resulting from in-situ damage surveys.

At detailed scale (Phase 2), the analysis focuses on structurally independent single buildings in order to associate the differential settlements, defined as the maximum difference of PSI-derived vertical settlement between two points of the foundation (see also Peduto et al., 2016b, 2016c; Sanabria et al., 2014), with the damage severity recorded on each building and grouped according to the building foundation typology. Finally, PSI-derived differential settlements are assumed as intensity parameter for the generation of empirical fragility curves for single buildings resting on both shallow and deep foundations.

5. Study area and available datasets

The proposed methodology was applied to densely urbanized areas in the south-west portion of The Netherlands (Figs. 2a, 2b, 2c) where the subsoil includes highly compressible clayey and peaty soil layers extending to depths of about 15-20 m. The built-up area presents different building typologies, mainly masonry structures, resting on different foundation types (e.g. shallow or piled foundations). The analysis was carried out at medium scale over an area of about 15 km^2 and including the cities of Rotterdam and Schiedam (Fig. 2a). Then, the analysis at large scale focused on a smaller area of about 2 km^2 represented by a neighborhood of Schiedam (Fig. 2b); at detailed scale, a portion of the neighborhood of Schiedam (Fig. 2c) including 310 structurally independent buildings was considered.

This is a post-peer-review, pre-copyedit version of an article published in **ENGINEERING GEOLOGY**. The final authenticated version is available online at: **http://dx.doi.org/10.1016/j.enggeo.2016.12.018**

5.1 Geological context

The Netherlands is predominantly a flat country; about 60% of shallow soil deposits are of Holocene age and of fluvial and coastal origin. The sediments of coastal origin have their current ground surface elevations at or below the mean sea level. The eastern part of the country consists almost entirely of Pleistocene deposits, mainly constituted by sandy soils sloping upwards to the south (van der Meulen et al., 2013). Since the 1960s onward, the Geological Survey of the Netherlands (TNO) started a detailed geological mapping program focused on the southwestern part of The Netherlands. This activity provided a database of maps at 1:50,000 scale along with vertical cross-sections (Hageman, 1964; van Rummelen, 1965, 1972; Vos and Van Heeringen, 1997). More recently, TNO has built the 3D geological 'GeoTOP' model (DINOloket, 2016) that represents a sound basis on properties and features of the national subsoil. The model, which extends down to a depth of 50 m below the ground surface with almost a nationwide coverage, schematizes the national territory in millions of voxels, each measuring 100 × 100 × 0.5 m (height × width × depth). Each voxel contains information on the litho-stratigraphy (including the probability of occurrence of each lithological class) as a result of a systematic collection and analysis of hundreds of thousands borehole data and cone penetration tests (Stafleu et al., 2011).

With reference to the study area, GeoTOP-derived information was used to generate the land cover map (Fig. 3a), the cumulative thickness maps for soft (Fig. 3b) and sandy soils (Fig. 3c). Figure 3d shows a typical section with soft soil layers of Holocene age – with total thicknesses not exceeding 20 m – superimposed on a sandy layer of similar thickness. Below, soft soils including narrow lenses of sandy soils rests on a sandy deposit of Pleistocene age.

Hoogland et al. (2011) demonstrated that the subsidence rate of peaty and non-peaty soils in the eastern area of Amsterdam, Utrecht, Rotterdam and Den Haag would exceed 80 mm

This is a post-peer-review, pre-copyedit version of an article published in **ENGINEERING GEOLOGY**. The final authenticated version is available online at: **http://dx.doi.org/10.1016/j.enggeo.2016.12.018**

between 2005 and 2020. This requires special attention on the effects that these settlements may produce to buildings and infrastructures, in order to develop appropriate strategies in land use planning and management of the built-up areas.

5.2 PS-InSAR data

The available SAR dataset over the study area consists of 285 images (133 from the ascending orbit and 162 from the descending orbit) acquired by the TerraSAR-X (TSX) constellation of satellites in the time spanning 2009–2014 (Table 1). These data were processed by SkyGeo Netherlands B.V. using their commercial processing chain 'Antares', which implements the PSI method described in Ferretti et al. (2001) and a great number of state-of-art improvements and complementary techniques. As an input DEM, the SRTM90 (e.g. USGS, 2016) was used. Considering the flatness of Dutch topography, this resolution is sufficient to reach the desired precision. The resulting PSI velocity measurements passed a quality assurance protocol from which the measurement precision shown in Table 2 was derived for both datasets using the ascending and the descending orbit images.

For purposes of easier analysis the PSI data were projected from the LOS to the vertical direction (Cascini et al., 2007) since subsidence-related displacements were assumed as mainly vertical. In theory, data from the ascending and descending directions can be combined to derive the vertical deformation component (Manzo et al., 2006; Peduto et al., 2015) with greater precision. In this case however, the method was not used as, via a comparison of the same PSI dataset with leveling benchmarks, Nicodemo et al. (2016) demonstrated that the assumption of verticality does not introduce significant errors as the total error is well below 1 mm/year.

This is a post-peer-review, pre-copyedit version of an article published in **ENGINEERING GEOLOGY**. The final authenticated version is available online at: **http://dx.doi.org/10.1016/j.enggeo.2016.12.018**

Furthermore, the data originating from the tops of buildings were separated from the data originating from ground level via the use of AHN2 (2016), a detailed and publicly available LiDAR-derived DEM of the Netherlands with a vertical precision of 5 cm at 50 cm resolution cells. Based on the analysis of the histograms of the heights, all PS heights less than 2 m above the DEM terrain height were assigned to the "ground level" class. Another source of error is, that PS can originate from the top of buildings or from the façade at different heights. Considering the geolocation precision of the PS, we did not attempt to correct for this. The errors introduced in this manner are so small that the total error is still less than 1 mm/yr, as shown in Nicodemo et al. (2016). However, the reader can refer to Tapete et al. (2015) to carry out the same operation in less favourable conditions as in the present study.

It can be noticed that Figures 4 a and 4 b (respectively showing PS on top of the buildings and at ground level), which were derived from the ascending dataset, and Figure 4 c and 4 d (respectively showing PS on top of the buildings and at ground level), which were derived from the descending dataset, exhibit almost similar velocity patterns independently of the acquisition geometry. Moreover, the high density coverage in the study area can be appreciated (7136 PS/km^2 on ascending orbit and 8793 PS/km^2 on descending orbit) thus confirming the improved capability of last generation X-band sensors in built-up area monitoring.

6. Results

6.1 Phase 0

As already highlighted, ground displacements associated with the viscous behavior of soft soil layers are generally highly variable in time and space according to both the spatial distribution

This is a post-peer-review, pre-copyedit version of an article published in **ENGINEERING GEOLOGY**. The final authenticated version is available online at: **http://dx.doi.org/10.1016/j.enggeo.2016.12.018**

of their cumulative thickness and their compressibility, in turn mainly related to the organic matter content and acting effective stresses (van Asselen et al., 2010). Therefore, in the study area, the role played by the factors predisposing to ground displacements was first investigated at medium scale (Fig. 2a) by recovering the relationship between the soft soil cumulative thickness and the PSI-derived settlement magnitude in free-field conditions. To this aim, only PSI data at ground level were considered. Then, according to both the scale of analysis (Fell et al., 2008; Peduto et al., 2015) and the accuracy of the available geological model, a grid was imposed on the area under investigation with a cell size of 100 × 100 m on which the vertical PSI velocities were interpolated using the Inverse Distance Weighting (IDW) method. The velocity values computed for each cell were then multiplied for the acquisition period of the radar sensor images, thereby generating the cumulative settlement maps shown in Figures 5a and 5b. It can be observed that cumulative settlements in the period 2009-2014 range up to 3 - 5 cm. In a few areas, coloured in red in Figures 5a and 5b, they even exceed 5 cm.

It is worth noting that the available piezometric measurements in the study area do not show significant changes over time so that the groundwater level can be assumed as a constant. This confirms that the recorded settlements in the study area can be merely ascribed to the intrinsic characteristics of the soft soil layers. Therefore, the PSI-derived settlement maps (Figs. 6a and 6c) were compared with the map of cumulative soft soil thickness (organic and clayey material) (Fig. 6e). After drawing a generic cross section (e.g. section A-A' in Figs. 6a, 6c and 6e) it can be observed that the maximum settlements (Figs. 6b and 6d) are recorded where the maximum cumulative thicknesses of soft soils (Fig. 6f) are present. In particular, this mainly occurs where the organic matter content increases in the soft soil layers (with probability of occurrence close to one, see Fig. 6g). For instance, this can be easily noticed in the first part

This is a post-peer-review, pre-copyedit version of an article published in **ENGINEERING GEOLOGY**. The final authenticated version is available online at: **http://dx.doi.org/10.1016/j.enggeo.2016.12.018**

of the diagram of Fig. 6h moving from A to A'. Conversely, where soft soil thicknesses are lower and the organic matter content decreases, lower PSI-derived settlements are recorded. As a result, the areas with the thickest cumulative soft soil layers and the highest settlements (red and orange areas in Figs. 5a and 5b) were confirmed to be the most affected by settlements. In these areas, the most severe consequences to structures and infrastructures are likely to be expected.

6.2 Phase 1

The analysis at large scale was carried out on a neighborhood of the city of Schiedam where mainly masonry buildings are present. The buildings are supported by different types of foundation, i.e. shallow and piled foundations. The available PSI-data show different values of the average velocities at ground level and on top of buildings, as highlighted in the 3D view of Figure 7. For instance, during the image acquisition period the vertical velocity values at ground level mostly range from -3 to -5 mm/year. Lower velocities are recorded on top of the buildings, mainly in those supported by foundations piled into stable Pleistocene sand layers.

In order to identify the buildings affected by settlements and analyze their behavior, PS data at ground level and on top of buildings were preliminarily used to differentiate the building aggregates and the areas surrounding the buildings that are “moving” from those that are “not moving”. To this aim, based on the available digital topographic map, building aggregates were identified with the row houses typical of the local architecture. For each building aggregate, all PS at roof level were selected considering a 2-meter buffer-distance around each building aggregate. The 2-meter buffer-distance is a practical consideration. Since the geolocation precision of the PS is less than 1.5 m, a large number of PS are projected outside

This is a post-peer-review, pre-copyedit version of an article published in **ENGINEERING GEOLOGY**. The final authenticated version is available online at: **http://dx.doi.org/10.1016/j.enggeo.2016.12.018**

of the building outlines, which themselves have a geolocation precision of circa 10 cm. In Dutch practice, there are only a few potential sources of irrelevant data within 2 m from a building façade, i.e. lighting poles. By using a 2-meter buffer-distance, many valid PS are included in the analysis, while only few invalid PS are introduced.

A "moving/not moving" conservative threshold of 2 mm/year was fixed taking into account that a validation test carried out by Nicodemo et al. (2016) with the same PSI-dataset over 180 leveling points in the Schiedam area revealed an average difference of about 0.67 mm/yr with a standard deviation of 0.48 mm/yr between the yearly average velocity derived from leveling and PSI data. The analysis showed that 33% of 648 building aggregates in the study area are covered by at least one "moving" PS (Fig. 7b). Similarly, the analysis of PS at ground level highlighted that 79% of the total area covered by roads and areas surrounding the buildings is moving (Fig. 7c).

Following the distinction of "moving/not moving" building aggregates and surrounding areas and roads, four possible scenarios were identified as cases C1-C4. Their description and spatial distribution are summarized in Figure 8. The above zoning of the study area allows the identification of portions of the territory where different problems may exist. For instance, if possible damages to roads and services are to be investigated, the analysis should focus on the parts of the territory belonging to classes C2, C3 and C4; conversely, if the analysis of building behaviour is addressed, only classes C3 and C4 are relevant. Overall, the analysis shows that 84% of the study area is affected by settlements, but only within 34% of it there might be buildings involved.

Once the areas where buildings are likely to be affected by settlement-related problems (C3 and C4) were identified, in-situ surveys were carried out in April and May of 2015. These surveys focused on the portion of Schiedam where damages had been recorded (Fig. 2c). The

This is a post-peer-review, pre-copyedit version of an article published in **ENGINEERING GEOLOGY**. The final authenticated version is available online at: **http://dx.doi.org/10.1016/j.enggeo.2016.12.018**

analysis of crack patterns exhibited by building façades can provide useful information in order to establish correlations between settlements and damage suffered by superstructures (Bianchini et al., 2015; Ferlisi et al., 2015; Palmisano et al., 2016; Peduto et al., 2016b, 2016c). In order to investigate both the severity and the distribution of damage to buildings, the surveyor used ad-hoc fact-sheets to capture this data. The fact-sheets consist of different sections that allow systematical recording of the archive information regarding the geological features and available settlement measurements as well as the information gathered from the in-situ surveys (Fig. 9), see also Pratesi et al. (2015a). Section 1 gathers information concerning the building location and its description in terms of structural type, foundation typology, number of floors, age of construction and occupancy type. The available datasets concerning the geological features and the PSI data are included in Section 2. Section 3 reports the photo collection of damage recorded on building façades such as the presence of cracks and/or disjunction in the outer walls and their position, as well as their distortion or tilt, and finally the assignment of the observed damage severity. The damage severity was differentiated in six levels: D0 = negligible; D1 = very slight; D2 = slight; D3 = moderate; D4 = severe; D5 = very severe. These Di (i = 0, …, 5) levels of damage severity are adapted from the classification proposed by Burland et al. (1977). In particular, D1-D2 levels refer to aesthetic damage characterized by hairline/fine cracks that can be easily treated during normal decoration or require easy repair work. Starting from D3 level, when moderate damages can occur, maintenance works are necessary. Once D4 and D5 levels are reached, there is a risk for building safety since the damage can affect its structural stability. According to the scale of analysis, the "equivalent damage" attributed to a certain building aggregate was estimated as the average level of damage severity – weighted according to the number of buildings per

This is a post-peer-review, pre-copyedit version of an article published in **ENGINEERING GEOLOGY**. The final authenticated version is available online at: **http://dx.doi.org/10.1016/j.enggeo.2016.12.018**

Di and approximated to the closer level – recorded on the group of structurally dependent single buildings composing the "row house" aggregate (Peduto et al., 2016c).

Figures 10a and 10b show the results of the survey campaign on 67 building aggregates characterized by masonry structures built on different foundation types (43% shallow foundations, 49% piled foundations and 8% unknown). The collected data highlighted that 39% aggregate buildings out of the total do not exhibit any damage, whereas 61% of all estimated equivalent damages do not exceed the D2 level (D1 = 49%; D2 = 12%).

Focusing on the surveyed building aggregates, the settlements and related gradients suffered by each of them were evaluated following the steps shown in Figure 11 for a sample aggregate. In particular, vertical PSI velocities on top of the buildings (Fig. 11a) were interpolated on a superimposed grid with cell sizes of 2 × 2 m using an IDW interpolation. Then, the velocity for each cell was multiplied for the acquisition period of the radar images in order to generate the cumulative settlement map for each building aggregate (Fig. 11b). Subsequently, since damage occurrence and severity for a given building is related to the magnitude of settlements, or their derived parameters describing foundation movements, the trend of settlements along the cross-section was evaluated (Fig. 11d). Then, starting from the measured cumulative settlements (Fig. 11b) the settlement gradient map (Fig. 11c) was generated and gradient moduli were grouped into the three classes (Low, Medium and High). In particular, these classes refer to the gradient values (expressed in degrees) which range respectively from 0 to 5.7×10^{-2} (corresponding to a differential settlement of 0 to 2 mm within the grid cell), from 5.7×10^{-2} to 1.4×10^{-1} (corresponding to a differential settlement of 2 to 5 mm within the grid cell) and greater than 1.4×10^{-1} (corresponding to a differential settlement greater than 5 mm within the grid cell). In the sample building aggregate in Figure 11, the settlement gradient profile (Fig. 11e) highlights rather low values with a maximum in

This is a post-peer-review, pre-copyedit version of an article published in **ENGINEERING GEOLOGY**. The final authenticated version is available online at: **http://dx.doi.org/10.1016/j.enggeo.2016.12.018**

the section indicated by the red arrow. This result was corroborated by the damage survey carried out in the area that revealed the presence of some cracks on the façades of the building with deformations of the sidewalk and detachments from the laying surface exactly at the location where the gradient peak is recorded (Fig. 9 – section 3 – pictures 3, 4 and 7).

Extending the same procedure to all 67 building aggregates, the maximum values of the settlement gradients were computed from the longitudinal profiles drawn along the settlement gradient maps. These values were then associated with the estimated equivalent damage, differentiating between building aggregates with shallow and deep foundations (Figs. 12a and 12b). The obtained results show a general increasing trend of the equivalent damage when the value of the maximum gradient increases for both foundation types (i.e. shallow and deep ones). This aspect was further investigated in the analysis at detailed scale carried out on single buildings.

6.3 Phase 2

The analysis at detailed scale focused on 310 single (or independent) buildings (see Fig. 13a) which correspond to the 67 "row houses" aggregates analyzed at large scale.

For each single building, the minimum (δv_{min}) and the maximum (δv_{max}) vertical settlement along the longitudinal cross-section (Fig. 13a) were computed on the cumulative settlement map. The differential settlement (Δ, Fig. 13b) was defined as the maximum difference of vertical settlement between any two points on the single building's foundation ($\delta v_{max} - \delta v_{min}$) (see also Sanabria et al., 2014). The obtained values were in turn correlated with the damage severity recorded for each building (Fig. 13a) in order to investigate the cause (differential settlements) and effect (recorded damage) relationship. Derived separately for shallow and piled foundations, a similar increasing trend of damage severity with the differential

This is a post-peer-review, pre-copyedit version of an article published in **ENGINEERING GEOLOGY**. The final authenticated version is available online at: **http://dx.doi.org/10.1016/j.enggeo.2016.12.018**

settlement was found for both foundation types (Figs. 13c and 13d). Note that in Figures 13c and 13d the damage severity ranges from D0 up to D3 levels, whereas the equivalent damage estimation on building aggregates (shown in Figures 12a and 12b) limited damage severity within the D0-D2 range.

Subsequently, under the assumption that the differential settlement is the representative intensity parameter of the natural event causing damage of different severity to the single buildings, empirical fragility curves were derived for a given foundation type and fixed differential settlement values. For this purpose, the frequency of occurrence of each level of damage severity was calculated for different classes of PSI-derived differential settlements (Figs. 14a and 14c). Then, using methods common in different engineering fields (Fotopoulou and Pitilakis, 2013; Mavrouli et al., 2014; Negulescu and Foerster, 2010; Negulescu et al., 2014; Pitilakis and Fotopoulou, 2015; Saeidi et al., 2009, 2012; Zhang and Ng, 2005), the probabilities were calculated using a cumulative log-normal distribution function:

$$P\left(\text{Damage} \geq \text{D}_\text{i} \middle| \Delta\right) = \Phi\left[\frac{1}{\beta} ln\left(\frac{\Delta}{\bar{\Delta}}\right)\right]$$

where $P(\cdot)$ is the probability of reaching or exceeding a particular level of damage severity D_i for a fixed intensity of differential settlement Δ; $\Phi[\_]$ is the standard normal cumulative distribution function; $\bar{\Delta}$ is the median value of Δ where the building reaches each D_i; and β is the standard deviation of the natural logarithm of Δ for each D_i. The median values of Δ, corresponding to each D_i, are those that give 50% probability of exceeding each level of damage severity; whereas the standard deviation β describes the variability associated with each fragility curve.

This is a post-peer-review, pre-copyedit version of an article published in **ENGINEERING GEOLOGY**. The final authenticated version is available online at: **http://dx.doi.org/10.1016/j.enggeo.2016.12.018**

The empirical fragility curves obtained for the surveyed masonry buildings with shallow and piled foundations are respectively shown in the Figures 14b and 14d, whereas the parameters of all computed fragility functions are synthesized in Table 3.

The Figures 14b and 14d highlight that, independently of the foundation type, for differential settlements lower than 9 mm the probability of reaching or exceeding the D3 (moderate) level of damage severity – often associated to losses of functionality – is negligible. Indeed, only damages whose severity (of D1 or D2 level) might affect the aesthetics – with different $P(\cdot)$ values according to the considered $\Delta \leq 9$ mm – are expected. Moreover, as the differential settlement increases (for Δ values larger than 9 mm), the probability of reaching or exceeding the D3 level increases more rapidly for buildings on shallow foundations (Fig. 14b) than those on piled foundations (Fig. 14d).

The reliability of the cumulative log-normal distribution function was checked using the Kolmogorov–Smirnov (K-S) goodness-of-fit test. In particular, the comparison between the calculated empirical fragility curves (Fo(x)) with the empirical distribution functions (FN(X)) defined in the K-S test (Fig.15) confirms that the assumption of the cumulative log-normal distribution function to describe the probability of exceeding a given level of damage severity is acceptable for all significance levels (from 1 to 20 %) taken as references. Indeed, as shown in Table 4, the absolute values of the maximum distances (D_{max}) between the considered log-normal distribution function for each level damage severity and the related empirical distribution function defined according to the K-S test are always lower than the critical values (D_{crit}) tabulated by Kolmogorov–Smirnov for different significance levels.

This is a post-peer-review, pre-copyedit version of an article published in **ENGINEERING GEOLOGY**. The final authenticated version is available online at: **http://dx.doi.org/10.1016/j.enggeo.2016.12.018**

7. Discussion and conclusions

The present work developed an integrated multi-scale approach for the analysis of the building response to ground settlements by combining information on the subsoil setting, PSI data and the results of damage surveys to buildings.

The preliminary analysis carried out at medium scale allowed confirming the role played by soft soils in predisposing the ground settlement occurrence in the selected urban area in The Netherlands. Although in the analyzed region monitoring data are properly archived in well-organized databases freely accessible to end-users, the availability of such a distributed displacement dataset as PSI data provided an unprecedented overview of the problems that the Dutch built-up environment usually has to face. The good match between the soft soil thickness map and the cumulative settlement map enabled to zone the areas that are most prone to ground surface lowering and, thus, where damages to the built-up environment are most likely to be found or expected.

As for the analysis at large scale, the preliminary identification of different scenarios for the exposed elements can be helpful for authorities in charge of land management in order to focus the attention on either structures or infrastructures (including utilities) for what concerns settlement-related consequences. Then, the relationship retrieved between cause (settlements) and effect (recorded damage) with reference to building aggregates provided an overview on their behavior depending on the foundation typology. In this regard, the results obtained in the city of Schiedam highlight that the equivalent damage recorded to building aggregates does not exceed the slight level (D2) for both shallow and deep foundations. These latter, while usually being able to reduce absolute settlements, suffer from higher settlement gradient values just in correspondence of the sections where the highest levels of building damage severity are recorded. This circumstance can be related to the peculiar foundation type of the

This is a post-peer-review, pre-copyedit version of an article published in **ENGINEERING GEOLOGY**. The final authenticated version is available online at: **http://dx.doi.org/10.1016/j.enggeo.2016.12.018**

examined buildings that are located in the study area. These buildings, built up from the beginning of the 19th century to the 1980s, present foundations consisting of both wooden and reinforced concrete piles. Decaying effects of the wood induced by both fungi and bacteria (Klaassen and Creemers, 2012: Peduto et al., 2016b), which inhibit capability of piles to reduce settlements, as well as the negative skin friction, which may affect the reinforced concrete piles in highly compressible materials not designed to respond to such effects, may cause loss of functionality of some piles with the onset of localized settlement gradients and consequent damage on the superstructure.

As for the analysis at detailed scale on 310 single buildings in Schiedam, the damage severity recorded during the survey campaign proved not to be as high as to cause concern for structure stability. This seems confirmed by low values of settlements and settlement gradients most likely related to secondary (creep) consolidation processes developing over very long times in the underlying soft soils.

However, it is necessary to underline that the damage recorded on many surveyed structures – although of low severity at present – has highlighted a structural suffering due to ground movements. This requires continuous settlement monitoring in order to implement appropriate mitigation strategies before the effects increase. In this case, a semi-empirical structural model for single-building damage assessment as the one developed with the use of DInSAR data by Arangio et al. (2013) could be helpful. As for the presented results, the empirical fragility curves derived for single buildings in the study area on both shallow and deep foundations, once further calibrated and validated, could support analysis and forecasting purposes. Indeed, taking into account that the considered structural and foundation typologies investigated in the present study well represent the local urban fabric of The Netherlands, the obtained empirical fragility curves, complemented by a fast automatized GIS

This is a post-peer-review, pre-copyedit version of an article published in **ENGINEERING GEOLOGY**. The final authenticated version is available online at: **http://dx.doi.org/10.1016/j.enggeo.2016.12.018**

procedure designed to derive intensity parameters from PSI data (e.g. settlements, settlement gradients and differential settlements), could be used in the management of settlement-affected built-up areas and also help in addressing restoration and adaptation policies for which large budgets are allocated every year.

It is worth stressing that the proposed procedure was tested under very favourable conditions (e.g. a flat area, good subsoil data, accurate LIDAR records, very high resolution SAR source data, extensive damage survey data and levelling measurements) and, accordingly, the quality of these data influenced the reliability of the obtained results. However, the presented fragility curves need to be further calibrated and validated before being used for forecasting purposes over similar areas where input data (except for DInSAR data and info/maps on buildings) are scarce. At the same time, the adopted approach holds the promise to be further enhanced thanks to a global trend towards open GIS data on housing and infrastructure as well as continuous improvements in the field of SAR sensors and PSI data processing that will allow an increase in data density, data precision and frequency of acquisition.

References

AHN2 (2016) Actueel Hoogtebestand Nederland 2. https://www.pdok.nl/nl/atomfeed/ahn2-05-meter-maaiveld-raster-opgevuld, in Dutch (accessed 28.10.2016).

Arangio, S., Calò, F., Di Mauro, M., Bonano, M., Marsella, M., Manunta, M., 2013. An application of the SBAS-DInSAR technique for the assessment of structural damage in the city of Rome, in Structure and Infrastructure Engineering: Maintenance, Management, Life-Cycle Design and Performance, Vol. 10, pp. 1469-1483, http://dx.doi.org/10.1080/15732479.2013.833949.

This is a post-peer-review, pre-copyedit version of an article published in **ENGINEERING GEOLOGY**. The final authenticated version is available online at: **http://dx.doi.org/10.1016/j.enggeo.2016.12.018**

Bandini, A., Berry, P., Boldini, D., 2015. Tunnelling-induced landslides: The Val di Sambro tunnel case study. Engineering Geology 196, 71-87.

Berardino, P., Fornaro, G., Lanari, R., Sansosti, E., 2002. A new algorithm for surface deformation monitoring based on small baseline differential SAR interferograms. IEEE Transaction on Geoscience and Remote Sensing 40 (11), 2375-2383.

Bianchini, S., Herrera, G., Mateos, R.M., Notti, D., Garcia, I., Mora, O., Moretti, S., 2013. Landslide activity maps generation by means of persistent scatterer interferometry. Remote Sensing 5(12), 6198-6222.

Bianchini, S., Pratesi, F., Nolesini, T., Casagli, N., 2015. Building Deformation Assessment by Means of Persistent Scatterer Interferometry Analysis on a Landslide-Affected Area: The Volterra (Italy) Case Study. Remote Sensing 7, 4678-4701.

Bjerrum, L., 1963. Allowable Settlement of Structures, in Proc. of the 3rd European Conference on Soil Mechanics and Foundation Engineering, Wiesbaden, 2, Brighton, England, pp. 135–137.

Boscardin, M.D., Cording, E.G., 1989. Building response to excavation induced settlement. Journal of Geotechnical Engineering 115, 1-21.

Burland, J.B., Broms B.B., De Mello V.F.B., 1977. Behaviour of foundations and structures, in SOA Report. Proc. 9th International Conference SMFE, Tokyo, Vol. 2, pp. 495-546.

Burland, J.B., Wroth, C.P., 1974. Settlement of Buildings and Associated Damage, in SOA Review. Proc. Conf. Settlement of Structures. Pentech Press, Cambridge, London, pp. 611–654.

Calò, F., Ardizzone, F., Castaldo, R., Lollino, P., Tizzani, P., Guzzetti, F., Lanari, R., Angeli, M.C., Pontoni, F., Manunta, M., 2014. Enhanced landslide investigations through advanced A-DInSAR techniques: the Ivancich case study, Assisi, Italy. Remote Sensing of Environment 142, 69-82.

Calò, F., Calcaterra, D., Iodice, A., Parise,M., Ramondini,M., 2012. Assessing the activity of a large landslide in southern Italy by ground-monitoring and SAR interferometric techniques. International Journal of Remote Sensing 33 (11), 3512-3530.

Carnec, C., King, C., Massonnet, D., 1995. Measurement of land subsidence by means of differential S.A.R. Interferometry to sites of small extent. Geophysical Research Letters 23, 3579-3582.

This is a post-peer-review, pre-copyedit version of an article published in **ENGINEERING GEOLOGY**. The final authenticated version is available online at: **http://dx.doi.org/10.1016/j.enggeo.2016.12.018**

Cascini, L., Di Maio C., 1994. Emungimento delle acque sotterranee e cedimenti nell'abitato di Sarno: analisi preliminare. Italian Geotechnical Journal XLI (3), 217-231(in Italian).

Cascini, L., Ferlisi, S., Fornaro, G., Lanari, R., Peduto, D., Zeni, G., 2006. Subsidence monitoring in Sarno urban area via multitemporal DInSAR technique. International Journal of Remote Sensing 27, 1709-1716.

Cascini, L., Ferlisi, S., Peduto, D., Fornaro, G., Manunta, M. 2007. Analysis of a subsidence phenomenon via DInSAR data and geotechnical criteria. Italian Geotechnical Journal XLI (4), 50-67.

Cascini, L., Peduto, D., Pisciotta, G., Arena, L., Ferlisi, S., Fornaro, G., 2013a. The combination of DInSAR and facility damage data for the updating of slow-moving landslide inventory maps at medium scale. Natural Hazards and Earth System Sciences 13, 1527-1549.

Cascini, L., Peduto, D., Reale, D., Arena, L., Ferlisi, S., Verde, S., Fornaro, G., 2013b. Detection and monitoring of facilities exposed to subsidence phenomena via past and current generation SAR sensors. Journal of Geophysics and Engineering 10(6), 064001.

Catalano, S., Bonforte, A., Guglielmino, F., Romagnoli, G., Tarsia, C., Tortorici, G., 2014. The influence of erosional processes on the visibility of Permanent Scatterers Features from SAR remote sensing on Mount Etna (E Sicily). Geomorphology 198, 128-137.

Cigna, F., Osmanoglu, B., Dixon, T.H., De Mets, C., Wdowinski, S., 2012. Monitoring land subsidence and its induced geological hazard with synthetic aperture radar interferometry: a case study in Morelia, Mexico. Remote Sensing of Environment 117, 46-161.

Cooper, A.H., 2008. The classification, recording, databasing and use of information about building damage caused by subsidence and landslides. Quarterly Journal of Engineering Geology and Hydrogeology 41(3), 409-424, 10.1144/1470-9236/07-223.

Costantini, M., Falco, S., Malvarosa, F., Minati F., 2008. A new method for identification and analysis of persistent scatterers in series of SAR images, in: IEEE International Geoscience & Remote Sensing Symposium, July 6–11, 2008, Boston, Massachusetts, USA, pp. 449–452.

Costantini, M., Falco, S., Malvarosa, F., Minati, F., Trillo, F., Vecchioli, F., 2014. Persistent scatterer pair interferometry: approach and application to high-resolution COSMOSkyMed SAR data. IEEE Journal of Selected Topics in Applied of Earth Observations and Remote Sensing 7, 2869-2878.

This is a post-peer-review, pre-copyedit version of an article published in **ENGINEERING GEOLOGY**. The final authenticated version is available online at: **http://dx.doi.org/10.1016/j.enggeo.2016.12.018**

Crosetto, M., Biescas, E., Duro, J., 2008. Generation of advanced ERS and Envisatinterferometric SAR products using the stable point network technique. Photogrammetric Engineering & Remote Sensing 4, 443-450.

Crosetto, M., Crippa, B., Biescas, E., 2005. Early detection and in-depth analysis of deformation phenomena by radar interferometry. Engineering Geology 79, 81-91.

Den Haan, E.J., Kruse, G.A.M., 2006. Characterisation and Engineering Properties of Dutch Peats, in: Tan, T.S., Phoon, K.K., Hight, D.W. and Leroueil, S. (Eds.), Characterisation and Engineering Properties of Natural Soils. Taylor & Francis Group, London, 3, pp. 2101-33.

DINOloket, 2016. Data and Information on the Dutch Subsurface. Open data portal of the Geological Survey of the Netherlands. https://www.dinoloket.nl/en (accessed 28.10.2016).

Fell, R., Corominas, J., Bonnard, Ch., Cascini, L., Leroi, E., Savage, W.Z., 2008. On behalf of the JTC-1 Joint Technical Committee on Landslides and Engineered Slopes. Guidelines for landslide susceptibility, hazard and risk zoning for land-use planning, Commentary. Engineering Geology 102, 99-111.

Ferlisi, S., Peduto, D., Gullà, G., Nicodemo, G., Borrelli, L., Fornaro, G., 2015. The use of DInSAR data for the analysis of building damage induced by slow-moving landslides, in G. Lollino et al. (Eds.), Engineering Geology for Society and Territory, Springer International Publishing Switzerland, Vol. 2, pp.1835-1839, DOI: 10.1007/978-3-319-09057.

Ferretti, A., Prati, C., Rocca, F., 2000. Nonlinear subsidence rate estimation using permanent scatterers in differential SAR interferometry. IEEE Transactions on Geoscience and Remote Sensing 38(5), 2202-2212.

Ferretti, A., Prati, C., Rocca, F., 2001. Permanent scatterers in SAR interferometry. IEEE Transactions on Geoscience and Remote Sensing 39 (1), 8-20.

Fornaro, G., Reale, D., Serafino, F. 2009. Four-dimensional SAR imaging for height estimation and monitoring of single and double scatterers. IEEE Transactions on Geoscience and Remote Sensing 47 (1), 212-237.

Fornaro, G., Reale, D., Verde, S., 2012. Potential of SAR for monitoring transportation infrastructures: an analysis with the multi-dimensional imaging technique. Journal of Geophysics and Engineering 9, S1.

Fornaro, G., Reale, D., Verde, S., 2013. Bridge thermal dilation monitoring with millimeter sensitivity via multidimensional SAR imaging. IEEE Geoscience and Remote Sensing Letters 10, 677–68.

This is a post-peer-review, pre-copyedit version of an article published in **ENGINEERING GEOLOGY**. The final authenticated version is available online at: **http://dx.doi.org/10.1016/j.enggeo.2016.12.018**

Fornaro, G., Pauciullo, A., Reale, D., Verde, S., 2014a. Multilook SAR Tomography for 3-D Reconstruction and Monitoring of Single Structures Applied to COSMO-SKYMED Data, in IEEE Journal of Selected Topics in Applied Earth Observations and Remote Sensing 7(7), 2776-2785.

Fornaro, G., Reale, D., Verde, S., Peduto, D., Arena, L., Ferlisi, S., 2014b. Potentialities of the use of spaceborne radar systems in the monitoring of structures and infrastructures, in: IEEE Workshop on Environmental Energy and Structural Monitoring Systems (EESMS), Naples, 17–18 September 2014, pp. 69–72, http://dx.doi.org/10.1109/EESMS.2014. 6923267

Fornaro, G., Verde, S., Reale, D., Pauciullo, A., 2015. CAESAR: An Approach Based on Covariance Matrix Decomposition to Improve Multibaseline–Multitemporal Interferometric SAR Processing, in: IEEE Transactions on Geoscience and Remote Sensing 53(4), 2050-2065.

Fotopoulou, S.D., Pitilakis, K.D., 2013. Fragility curves for reinforced concrete buildings to seismically triggered slow-moving slides. Soil Dynamics and Earthquake Engineering 48, 143-161.

Gernhardt, S., Adam, N., Eineder, M., Bamler, R., 2010. Potential of very high resolution SAR for persistent scatterer interferometry in urban areas. Ann. GIS 16(2), 103-111.

Giannico, C., Ferretti, A., Alberti, S., Jurina, L., Ricci, M., Sciotti, A., 2012. Application of satellite radar interferometry for structural damage assessment and monitoring Life-Cycle and Sustainability of Civil Infrastructure Systems: IALCCE'12, in: Strauss, A., Frangopol, D.M., Bergmeister, K. (Eds.), Proc. of the 3rd International Symposium on Life-Cycle Civil Engineering (Vienna, Austria, 3–6 Oct.), Boca Raton, FL: CRC Press, pp. 2094–101.

Gullà, G., Peduto, D., Borrelli, L., Antronico, L., Fornaro, G., 2016. Geometric and kinematic characterization of landslides affecting urban areas: the Lungro case study (Calabria, southern Italy). Landslides (in press), pp. 1-18, DOI: 10.1007/s10346-015-0676-0.

Hageman, B.P., 1964. BladGoeree en Overflakkee, Toelichtingbij de GeologischeKaart van Nederland, 1:50.000. RijksGeologischeDienst Haarlem, pp. 89 (in Dutch).

Hanssen, F.R. 2003. Subsidence monitoring using contiguous and PS-INSAR: Quality assessment based on precision and reliability in: Proc. 11th FIG Symposium on Deformation Measurements, Santorini, Greece, pp.1-8.

This is a post-peer-review, pre-copyedit version of an article published in **ENGINEERING GEOLOGY**. The final authenticated version is available online at: **http://dx.doi.org/10.1016/j.enggeo.2016.12.018**

Herrera, G., Fernandez-Merodo, J., Tomas, R., Cooksley, G., Mulas, J., 2009a. Advanced interpretation of subsidence in Murcia (SE Spain) using A-DInSAR data-modelling and validation. Natural Hazard and Earth System Sciences 9, 647-661.

Herrera, G., Gutiérrez, F., García-Davalillo, J.C., Guerrero, J., Notti, D., Galve, J.P., Fernández-Merodo, J.A., Cooksley, G., 2013. Multi-sensor advanced DInSAR monitoring of very slow landslides: the Tena Valley case study (Central Spanish Pyrenees). Remote Sensing of Environment 128, 31–43.

Herrera, G., Tomas, R., Lopez-Sanchez, J.M., Delgado, J., Vicente, F., Mulas, J., Cooksley, G., Sanchez, M., Duro, J., Arnaud, A., Blanco, P., Duque, S., Mallorqui, J.J., De la Vega-Panizo, R., Monserrat, O., 2009b. Validation and comparison of advanced differential interferometry techniques: Murcia metropolitan area case study. ISPRS Journal of Photogrammetry and Remote Sensing 64(5), 501-512.

Herrera, G., Tomas, R., Vicente, F., Lopez-Sanchez, J.M., Mallorqui, J.J., Mulas, J., 2010. Mapping ground movements in open pit mining areas using differential SAR interferometry. International Journal of Rock Mechanics and Mining Sciences 47(7), 1114-1125.

Holzer, T.L., 2009. Living with Unstable Ground. American Geosciences Institute publication - Environmental awareness series, pp. 68, ISBN: 0-922152-82-9 978-0-922152-82-7.

Hoogland, T., van den Akker, J.J.H., Brus, D.J., 2011. Modeling the Subsidence of Peat Soils in the Dutch Coastal Area. Geoderma 171-172, 92-97.

Huat, B.B.K., 2004. Organic and Peat Soils Engineering. University Putra Malaysia Press, Serdang, Malaysia, pp. 20-80.

Klaassen, R.K.W.M., Creemers, J.G.M. 2012. Wooden foundation piles and its underestimated relevance for cultural heritage. Journal of Cultural Heritage 13, 123-128.

Lee, C.W., Lu, Z., Won, J.S., Jung, H.S., Dzurisin, D., 2013. Dynamic deformation of Seguam Island, Alaska, 1992–2008, from multi-interferogram InSAR processing. Journal Volcanology and Geothermal Research 260, 43-51.

Manzo, M., Ricciardi, G.P., Casu, F., Ventura, G., Zeni, G., Borgstrom, S., Berardino, P., Del Gaudio, C., Lanari, R., 2006. Surface deformation analysis in the Ischia Island (Italy) based on spaceborne radar interferometry. Journal Volcanology and Geothermal Research 151(4), 399-416.

Mavrouli, O., Fotopoulou, S., Pitilakis, K., Zuccaro, G., Corominas, J., Santo, A., Cacace, F., De Gregorio, D., Di Crescenzo, G., Foerster, E., Ulrich, T., 2014. Vulnerability assessment

This is a post-peer-review, pre-copyedit version of an article published in **ENGINEERING GEOLOGY**. The final authenticated version is available online at: **http://dx.doi.org/10.1016/j.enggeo.2016.12.018**

for reinforced concrete buildings exposed to landslides. Bulletin of Engineering Geology and the Environment 73, 265-289, DOI: 10.1007/s10064-014-0573-0.

Negulescu, C., Foerster, E., 2010. Parametric studies and quantitative assessment of the vulnerability of a RC frame building exposed to differential settlements. Natural Hazard and Earth System Sciences 10(9), 1781–1792.

Negulescu, C., Ulrich, A., Seyedi, D.M., 2014. Fragility curves for masonry structures submitted to permanent ground displacements and earthquakes. Natural Hazards 74, 1461–1474, DOI: 10.1007/s11069-014-1253-x.

Nicodemo G., Peduto D., Ferlisi S., Maccabiani J., (2016) Investigating building settlements via very high resolution SAR sensors, in: Bakker, J., Frangopol, D.M., van Breugel, K. (Eds.) Life-Cycle of Engineering Systems: Emphasis on Sustainable Civil Infrastructure. Proceedings of the Fifth International Symposium on Life-Cycle Civil Engineering (IALCCE 2016), 16-19 October 2016, Delft, The Netherlands, Taylor & Francis Group, London, pp. 2256-2263.

Palmisano. F., Vitone, C., Cotecchia, F., 2016. Landslide damage assessment at the intermediate to small scale, in: Aversa, S., Cascini, L., Scavia, C. (Eds.), Landslides and Engineered Slopes. Experience, Theory and Practice, Vol. 1, pp. 1549-1557.

Pazzi, V., Morelli, S., Pratesi, F., Sodi T., Valori, L., Gambacciani, L., Casagli, N., 2016. Assessing the safety of schools affected by geo-hydrologic hazards: The geohazard safety classification (GSC), International Journal of Disaster Risk Reduction 15(2016), 80-93.

Peduto, D., Cascini, L., Arena, L., Ferlisi, S., Fornaro, G., Reale, D., 2015. A general fremework and related procedures for multi scale analyses of DInSAR data in subsiding urban areas. ISPRS Journal of Photogrammetry and Remote Sensing 105, 186-210, ISSN 0924-2716, http://dx.doi.org/10.1016/j.isprsjprs.2015.04.001.

Peduto, D., Huber, M., Speranza, G., van Ruijven, J., Cascini L., 2016a. DInSAR data assimilation for settlement prediction: case study of a railway embankment in The Netherlands. Canadian Geotechnical Journal, Published on the web 10 November 2016, DOI: 10.1139/cgj-2016-0425

Peduto, D., Nicodemo, G., Maccabiani, J., Ferlisi, S., D'Angelo, R., Marchese, A., 2016b. Investigating the behaviour of buildings with different foundation types on soft soils: two case studies in The Netherlands. VI Italian Conference of Researchers in Geotechnical Engineering, CNRIG2016 - Geotechnical Engineering in Multidisciplinary Research: from Microscale to Regional Scale, 22-23 September 2016, Bologna (Italy). Procedia Engineering 158(2016), 529-534, http://dx.doi.org/10.1016/j.proeng.2016.08.484

This is a post-peer-review, pre-copyedit version of an article published in **ENGINEERING GEOLOGY**. The final authenticated version is available online at: **http://dx.doi.org/10.1016/j.enggeo.2016.12.018**

Peduto, D., Pisciotta, G., Nicodemo, G., Arena, L., Ferlisi, S., Gullà, G., Borrelli, L., Fornaro, G., Reale, D., 2016c. A procedure for the analysis of building vulnerability to slow-moving landslides, in: Daponte, P., Simonelli, A.L. (Eds.), Proceedings of the 1st IMEKO TC4 International Workshop on Metrology for Geotechnics – Benevento, Italy, March 17-18, 2016 – pp. 248-254, ISBN: 978-92-990075-0-1.

Perissin, D., Prati, C., Rocca, F., 2009. PSInSAR analysis over the three gorges dam and urban areas in China. Urban Remote Sensing Joint Event, 2009 Joint, pp. 1-5.

Pitilakis, K., Fotopoulou, S., 2015. Vulnerability assessment of buildings exposed to co-seismic permanent slope displacements, in: Proc. of the XVI ECSMGE Geotechnical Engineering for Infrastructure and Development, pp. 151-153, ISBN 978-0-7277-6067-8, DOI: 10.1680/ecsmge.60678.

Polshin, D.E., Tokar, R.A., 1957. Maximum Allowable Non-uniform Settlement of Structures, in Proc. of the 4th International Conference on Soil Mechanics and Foundation Engineering, London, Vol. 1, pp. 402–405.

Pratesi, F., Tapete, D., Terenzi, G., Del Ventisette C., Moretti, S., 2015a. Structural Assessment of Case Study Historical and Modern Buildings in the Florentine Area Based on a PSI-Driven Seismic and Hydrogeological Risk Analysis, in: Lollino, G., Giordan, D., Marunteanu, C., Christaras, B., Yoshinori, I., Margottini, C., (Eds.), Engineering Geology for Society and Territory. Springer International Publishing Switzerland, Vol. 8, pp. 345-349, DOI: 10.1007/978-3-319-09408-3_60.

Pratesi, F., Tapete, D., Terenzi, G., Del Ventisette C., Moretti, S., 2015b. Rating health and stability of engineering structures via classification indexes of InSAR Persistent Scatterers. International Journal of Applied Earth Observation and Geoinformation 40 (2015), 81–90.

Prati, C., Ferretti, A., Perissin, D., 2010. Recent advances on surface ground deformation measurement by means of repeated space-borne SAR observations. Journal of Geodynamics 49, 161-170, http://dx.doi.org/10.1016/j.jog.2009.10.011.

Raucoles, D., Maisons, C., Carnec, C., Le Mouelic, S., King, C., Hosford, S., 2003. Monitoring of slow ground deformation by ERS radar interferometry on the Vauvert salt mine (France). Comparison with ground-based measurement. Remote Sensing of Environment 88, 468-478.

Reale, D., Fornaro, G., Pauciullo, A., Zhu, X., Bamler, R., 2011. Tomographic imaging and monitoring of buildings with very high resolution SAR data. IEEE Geoscience and Remote Sensing Letters 8, 661-665.

This is a post-peer-review, pre-copyedit version of an article published in **ENGINEERING GEOLOGY**. The final authenticated version is available online at: **http://dx.doi.org/10.1016/j.enggeo.2016.12.018**

Saeidi, A., Deck, O., Verdel, T., 2009. Development of building vulnerability functions in subsidence regions from analytical methods. Engineering Structures 31, 2275-2286.

Saeidi, A., Deck, O., Verdel, T., 2012. Development of building vulnerability functions in subsidence regions from analytical methods. Geotéchnique 62(2), 107-120.

Sanabria, M.P., Guardiola-Albert, C., Tomas, R., Herrera, G., Prieto, A., Sanchez, H., Tessitore, S., 2014. Subsidence activity maps derived from DInSAR data: Orihuela case study. Natural Hazards and Earth System Sciences 14, 1341–1360.

Skempton A.W., MacDonald D.H., 1956. Allowable Settlement of Buildings, in Proc. of the ICE (Institute of Civil Engineers), Vol. 5, Pt. III, pp. 727–768.

Stafleu, J., Maljers, D., Gunnink, J.L.,Menkovic, A., Busschers, F.S., 2011. 3D modeling of the shallow subsurface of Zeeland, the Netherlands. Netherlands Journal of Geosciences – Geologie en Mijnbouw 90-4, 293-310.

Tapete, D., Morelli, S., Fanti, R., Casagli, N., 2015. Localising deformation along the elevation of linear structures: An experiment with space-borne InSAR and RTK GPS on the Roman Aqueducts in Rome, Italy. Applied Geography 58(2015), 65-83, http://dx.doi.org/10.1016/j.apgeog.2015.01.009.

Tofani, V., Raspini, F., Catani, F., Casagli, N., 2014. Persistent scatterer interferometry (PSI) technique for landslide characterization and monitoring, in Sassa, K., Canuti, P., Yueping, Y. (eds.), Landslide Science for a Safer Geoenvironment, Vol. 2, Methods of Landslide Studies. Springer International Publishing, pp. 351–357, ISBN: 9783319050492.

Tomás, R., Cano, M., Garcia-Barba, J., Vicente, F., Herrera, G., Lopez-Sanchez, J.M., 2013. Monitoring an earth fill dam using differential SAR interferometry: La Pedrera dam, Alicante, Spain. Engineering Geology 157, 21-32.

Tomás, R., Romero, R., Mulas, J., Marturia, J.J., Mallorqui, J.J., Lopez-Sanchez, J.M., Herrera, G., Gutierrez, F., Gonzalez, P.J., Fernandez Torres, J., Duque, S., Concha- Dimas, A., Cocksley, G., Castaneda del Alamo, C., Carrasco, D., Blanco, P., 2014. Radar interferometry techniques for the study of ground subsidence phenomena: a review of practical issues through cases in Spain. Environmental Earth Sciences 71(1), 163-181.

USGS, 2016. http://dds.cr.usgs.gov/srtm/ (accessed 28.10.2016).

van Asselen, S., Stouthamer, E., Smith, N.D., 2010. Factors controlling peat compaction in alluvial floodplains – A case study in the cold-temperature Cumberland Marshes, Canada.

Journal Sedimentary Research 80, 155-166.

van der Meulen, M.J., Doornenbal, J.C., Gunnink, J.L., Stafleu, J., Schokker, J., Varnes, R.W., van Geer, F.C., van Gessel, S.F., van Heteren, S., van Leeuwen, R.J.W., Bakker, M.A.J., Bogaard, P.J.F., Busschers, F.S., Griffiooen, J., Gruijters, S.H.L.L., Kiden, P., Schroot, B.M., Simmelink, H.J., van Berkel, W.O., van der Krogt, R.A.A., Westerhoff, W.E., van Daalen, T.M., 2013. 3D geology in a 2D country: perspectives for geological surveying in the Netherlands. Netherlands Journal of Geosciences – Geologie en Mijnbouw 92-4, 217-241.

van Rummelen, F.F.F.E., 1965. Zeeuwsch Vlaanderen, Bladen Zeeuwsch Vlaanderen, West en Oost, Toelichtingbij de Geologische Kaart van Nederland, 1:50.000. Rijks Geologische Dienst Haarlem, pp. 79 (in Dutch).

van Rummelen, F.F.F.E., 1972. Blad Walcheren, Toelichtingbij de Geologische kaart van Nederland 1:50.000. Rijks Geologische Dienst, Haarlem, pp. 120 (in Dutch).

van Westen, C.J., Castellanos Abella, E.A., Sekhar, L.K., 2008. Spatial data for landslide susceptibility, hazards and vulnerability assessment: an overview. Engineering Geology 102(3-4), 112-131.

Vos, P.C., Van Heeringen, R.M., 1997. Holocene geology and occupation history of the Province of Zeeland, in: Fischer, M.M. (Ed.), Holocene evolution of Zeeland (SW Netherlands), pp. 5-110.

Wasowski, J., Bovenga, F., 2014. Investigating landslides and unstable slopes with satellite multi temporal interferometry: current issues and future perspectives. Engineering Geology 174, 103–138.

Zhang, L.M., Ng, A.M.Y., 2005. Probabilistic limiting tolerable displacements for serviceability limit state design of foundations. Geotéchnique 55(2), 151-161

Zhu, X., Bamler, R., 2010. Very high resolution spaceborne SAR tomography in urban environment. IEEE Transactions on Geoscience and Remote Sensing 48, 4296-4308.

This is a post-peer-review, pre-copyedit version of an article published in **ENGINEERING GEOLOGY**. The final authenticated version is available online at: **http://dx.doi.org/10.1016/j.enggeo.2016.12.018**

Highlights

A multi-scale procedure to analyse settlement-induced building damage is proposed

Role of soft soils in predisposing the ground settlement occurrence is investigated

DInSAR and damage data are combined to derive settlement vs. damage relationships

Equivalent damage of building aggregates is related to maximum settlement gradients

Empirical fragility curves are derived for single buildings on different foundations

This is a post-peer-review, pre-copyedit version of an article published in **ENGINEERING GEOLOGY**. The final authenticated version is available online at: **http://dx.doi.org/10.1016/j.enggeo.2016.12.018**

List of Figure captions

Fig. 1. Flowchart of the methodology

Fig. 2. The study area: a) area analyzed for investigating factors predisposing to ground settlements at medium scale; b) the study area at large scale and c) the study area at detailed scale.

Fig. 3. Geological setting of the study area: a) land cover; b) cumulative thickness of soft soils (organic and clayey); c) cumulative thickness of sandy soils, and d) geological cross-section along the A-A' profile sketched in a) (extracted from the portal of the Geological Survey of the Netherland – DINOloket).

Fig. 4. Distribution of PSI data provided by the TerraSAR-X radar sensor projected along the vertical direction: PSI data on ascending orbit a) on top of the buildings and b) at ground level, PSI data on descending orbit c) on top of the buildings and d) at ground level.

Fig. 5. Map of cumulative settlements in the period (2009-2014) using TerraSAR-X data at street level along the vertical direction on a) ascending and b) descending orbit.

Fig. 6. Correlation between cumulative settlements derived by high-resolution TerraSAR-X data at street level and geological information: maps of spatial distribution on a) ascending and c) descending orbit; cross-section along A-A' profile of the cumulative settlements on b) ascending and d) descending orbit in the period (2009-2014); e) map of spatial distribution and f) cross-section along A-A' profile of soft soils (organic and clayey); h) geological cross-section along the A-A' profile and g) probability of occurrence of soft soil (organic and clayey) extracted from the portal of the Geological Survey of the Netherland – DINOloket.

Fig. 7. Analysis of high-resolution PSI data at large scale: a) 3D view of the study area at large scale with spatial distribution of PSI vertical velocities at ground level and on top of the buildings; b) moving and not moving building aggregates and c) areas/roads surrounding the buildings.

Fig. 8. Spatial distribution of different possible scenarios resulting from the correlation analysis between moving and not moving PSI located on top of the building aggregates and on area/roads surrounding the buildings.

Fig. 9. Building fact-sheet: (section 1) location area and building information; (section 2) background data related to the geological context and PSI velocities; (section 3) some photos of the field survey and damage severity.

Fig. 10. a) Map of surveyed building aggregates distinguished according to the recorded equivalent damage level and foundation type; b) distribution (in percentage) of foundation types and equivalent damage levels in the surveyed area.

This is a post-peer-review, pre-copyedit version of an article published in **ENGINEERING GEOLOGY**. The final authenticated version is available online at: **http://dx.doi.org/10.1016/j.enggeo.2016.12.018**

Fig. 11. Analysis of high-resolution PSI data at large scale: a) distribution of TerraSAR-X data on top of building aggregates; b) map of cumulative settlements and c) map of settlement gradients derived from TerraSAR-X data (period 2009-2014); d) cumulative settlements and e) settlement gradients along the A-B profile sketched in b) and c).

Fig. 12. Maximum settlement gradients and related equivalent damage levels for building aggregates with a) shallow and b) piled foundations.

Fig. 13. Analysis of high-resolution PSI data at detailed scale: a) map of cumulative settlements and damage severity recorded in 2015 damage surveys; b) scheme of differential settlement assessment on the single building; damage level vs. differential settlements for buildings with c) shallow and d) piled foundations.

Fig. 14. Results of PSI-derived differential settlements and damage survey relationship for single buildings at detailed scale: class frequency of the different levels of damage severity recorded to buildings with a) shallow and c) piled foundations; fragility curves generated by using the log-normal distribution for single buildings with b) shallow and d) piled foundations.

Fig. 15. Results of the K-S goodness-of-fit test of the log-normal distribution function used for the generation of fragility curves for buildings with a) shallow and b) piled foundations.

This is a post-peer-review, pre-copyedit version of an article published in **ENGINEERING GEOLOGY**. The final authenticated version is available online at: **http://dx.doi.org/10.1016/j.enggeo.2016.12.018**

Table 1. Main features of the TerraSAR-X datasets (processed by PSI technique) used for the analysis.

Sensor	Orbit direction	Period of acquisition	Nr. of images	Ground Resolution (m × m)	Incidence angle (°)
TerraSAR-X	Ascending	06/04/2009 – 29/09/2014	133	3 × 3	39.3
TerraSAR-X	Descending	08/04/2009 – 20/09/2014	162	3 × 3	24.1

Table 2. PSI measurement precision

Measurement	Precision achieved
Single displacement measurement	< 4 mm
Linear displacement velocity	< 1 mm/year
Geolocation precision (x,y,z)	1.5 m
Geocoding precision (x,y)	< 1 cm

Table 3. Median and standard deviation parameters of the lognormal distribution function used for each damage levels and distinguished according to the foundation type.

Damage level	Shallow foundations		Piled foundations	
	Median [mm]	Stand. dev. [β]	Median [mm]	Stand. dev. [β]
D1 (Very slight)	3.86	0.32	4.35	0.26

This is a post-peer-review, pre-copyedit version of an article published in **ENGINEERING GEOLOGY**. The final authenticated version is available online at: **http://dx.doi.org/10.1016/j.enggeo.2016.12.018**

D2 (Slight)	5.94	0.28	5.64	0.19
D3 (Moderate)	10.58	0.08	10.47	0.14

Table 4. Results of K-S test.

Damage level	**Shallow foundations**						
	D_{max}	**D_{crit} α = 0.01**	**D_{crit} α = 0.05**	**D_{crit} α = 0.10**	**D_{crit} α = 0.15**	**D_{crit} α = 0.20**	**Test $D_{max} < D_{crit}$**
D1 (Very slight)	**0.108**	0.356	0.294	0.264	0.246	0.231	ok
D2 (Slight)	**0.137**	0.320	0.27	0.240	0.220	0.210	ok
D3 (Moderate)	**0.147**	0.618	0.521	0.470	0.436	0.410	ok
	Piled foundations						
D1 (Very slight)	**0.083**	0.216	0.180	0.162	0.151	0.142	ok
D2 (Slight)	**0.063**	0.275	0.235	0.215	0.195	0.185	ok
D3 (Moderate)	**0.265**	0.669	0.454	0.510	0.424	0.446	ok

This is a post-peer-review, pre-copyedit version of an article published in **ENGINEERING GEOLOGY**. The final authenticated version is available online at: **http://dx.doi.org/10.1016/j.enggeo.2016.12.018**

Figure_1_revised

Click here to download high resolution image

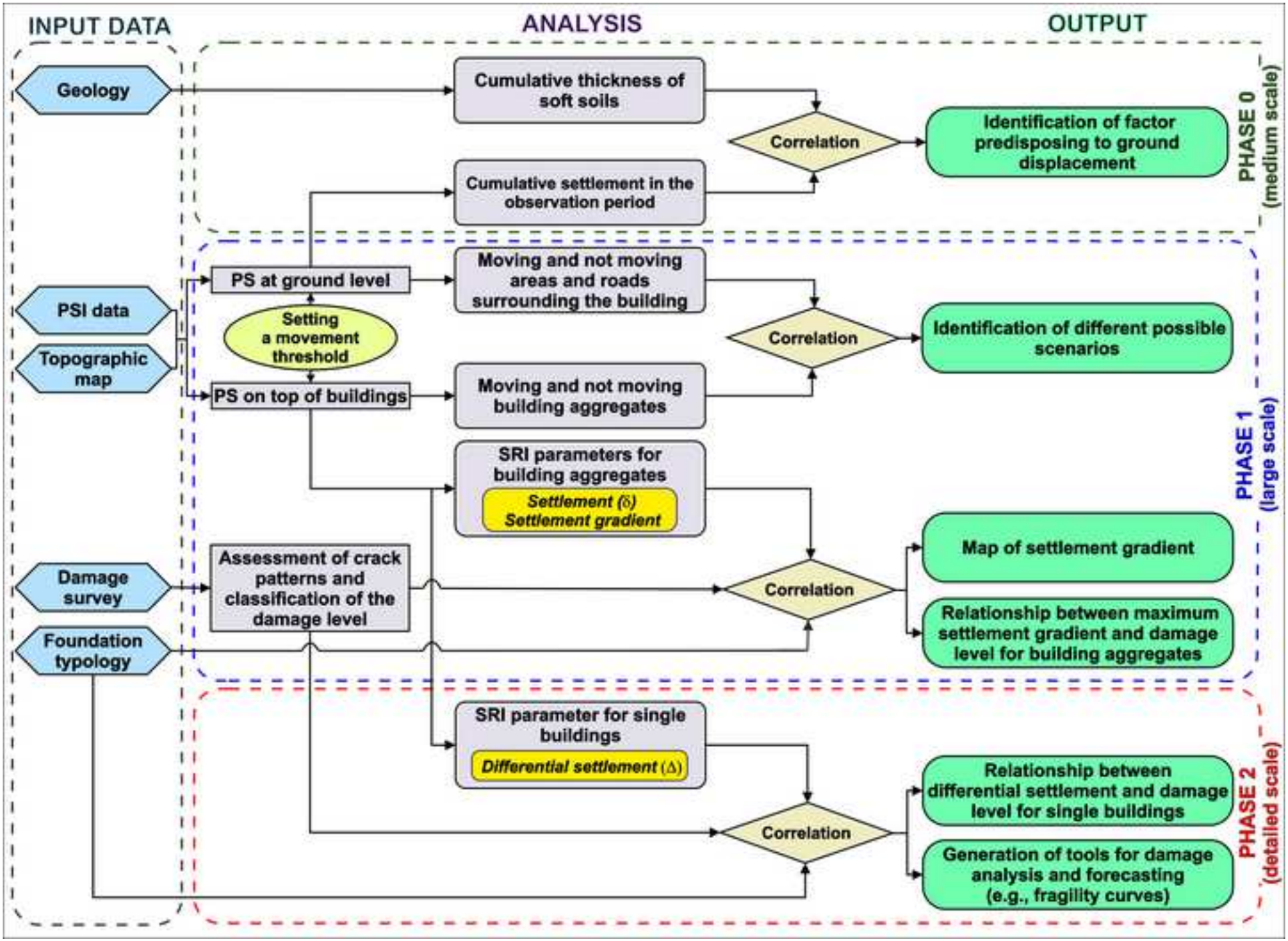

Figure_2_revised

Click here to download high resolution image

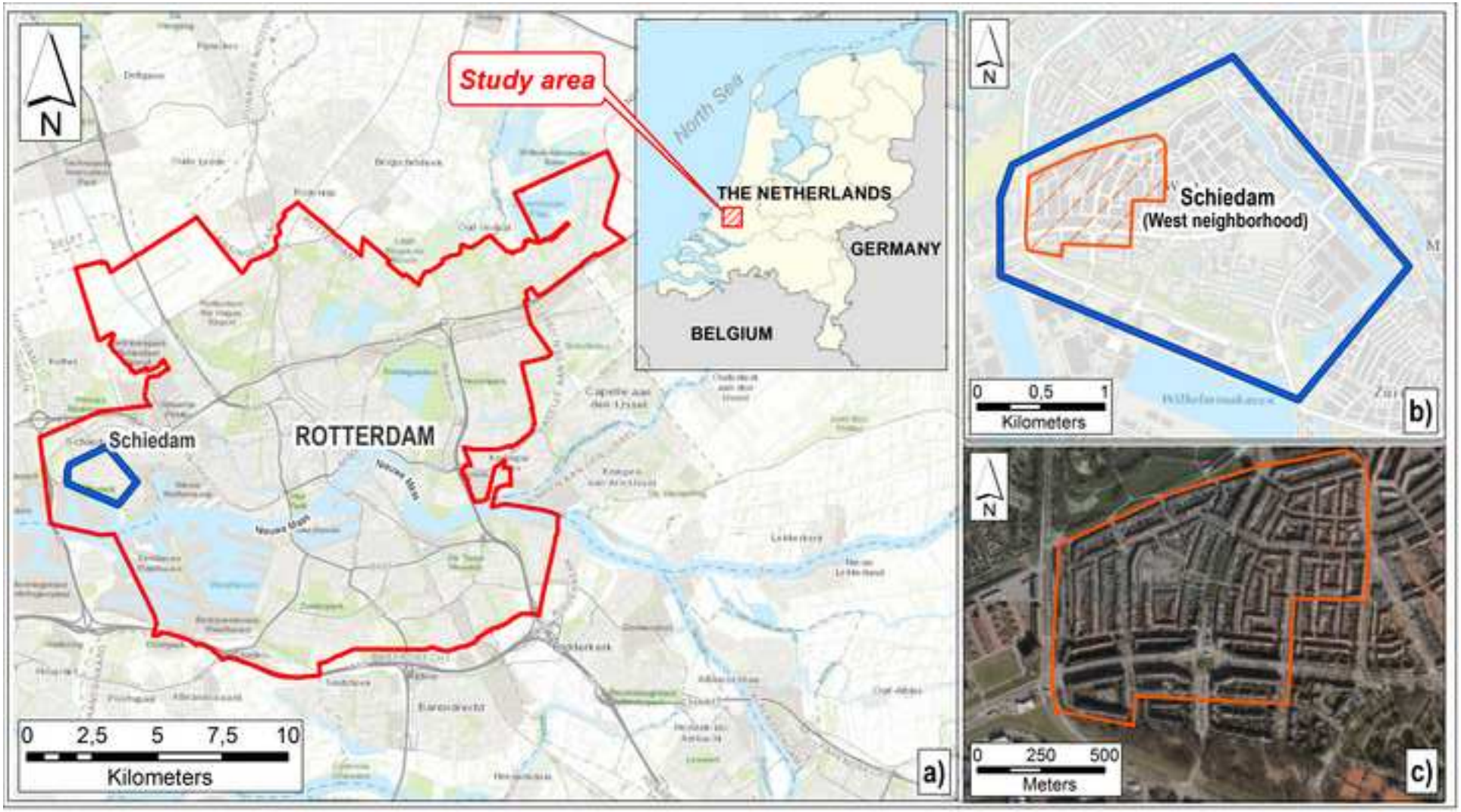

Figure_3_revised

Click here to download high resolution image

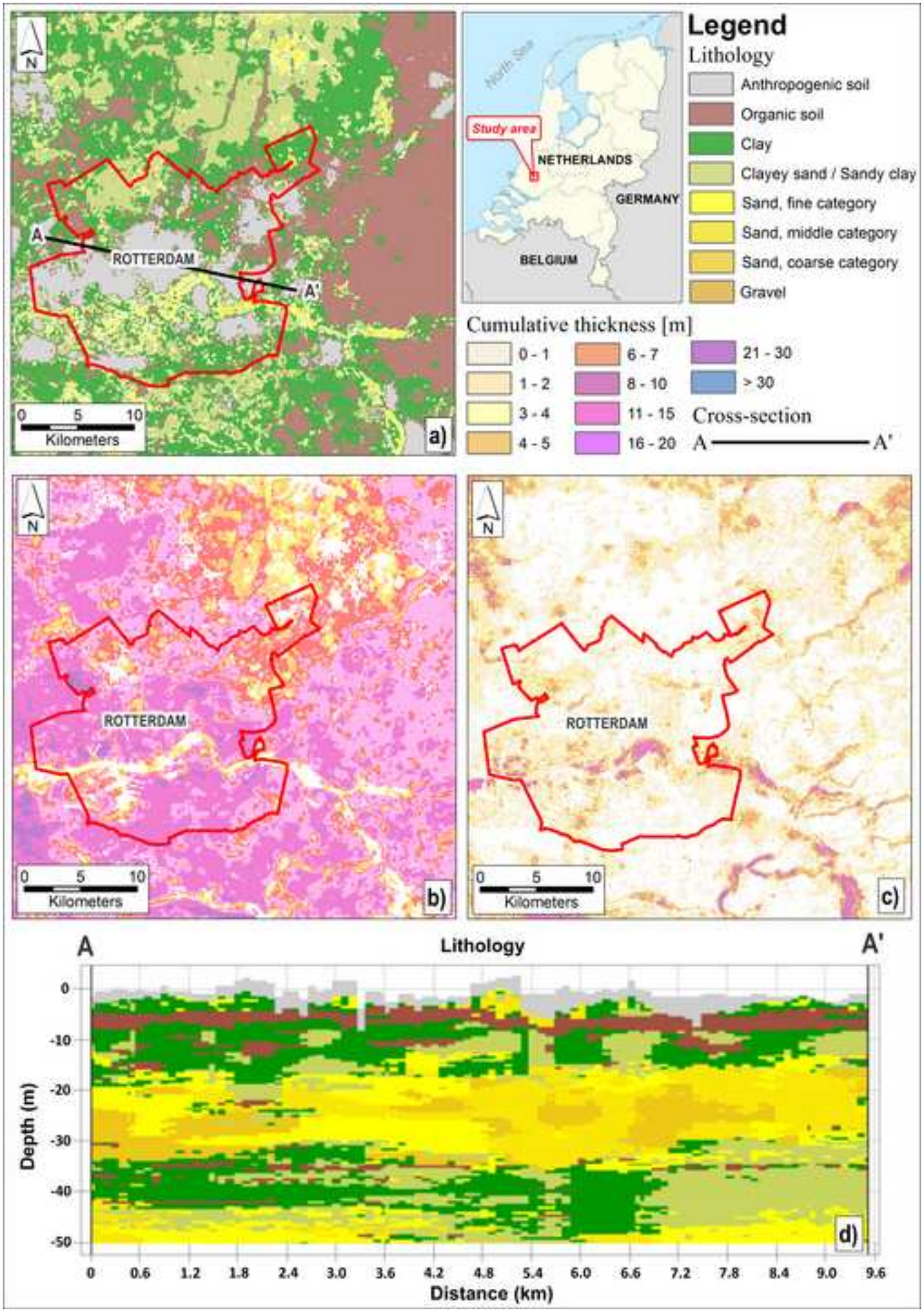

Figure_4
Click here to download high resolution image

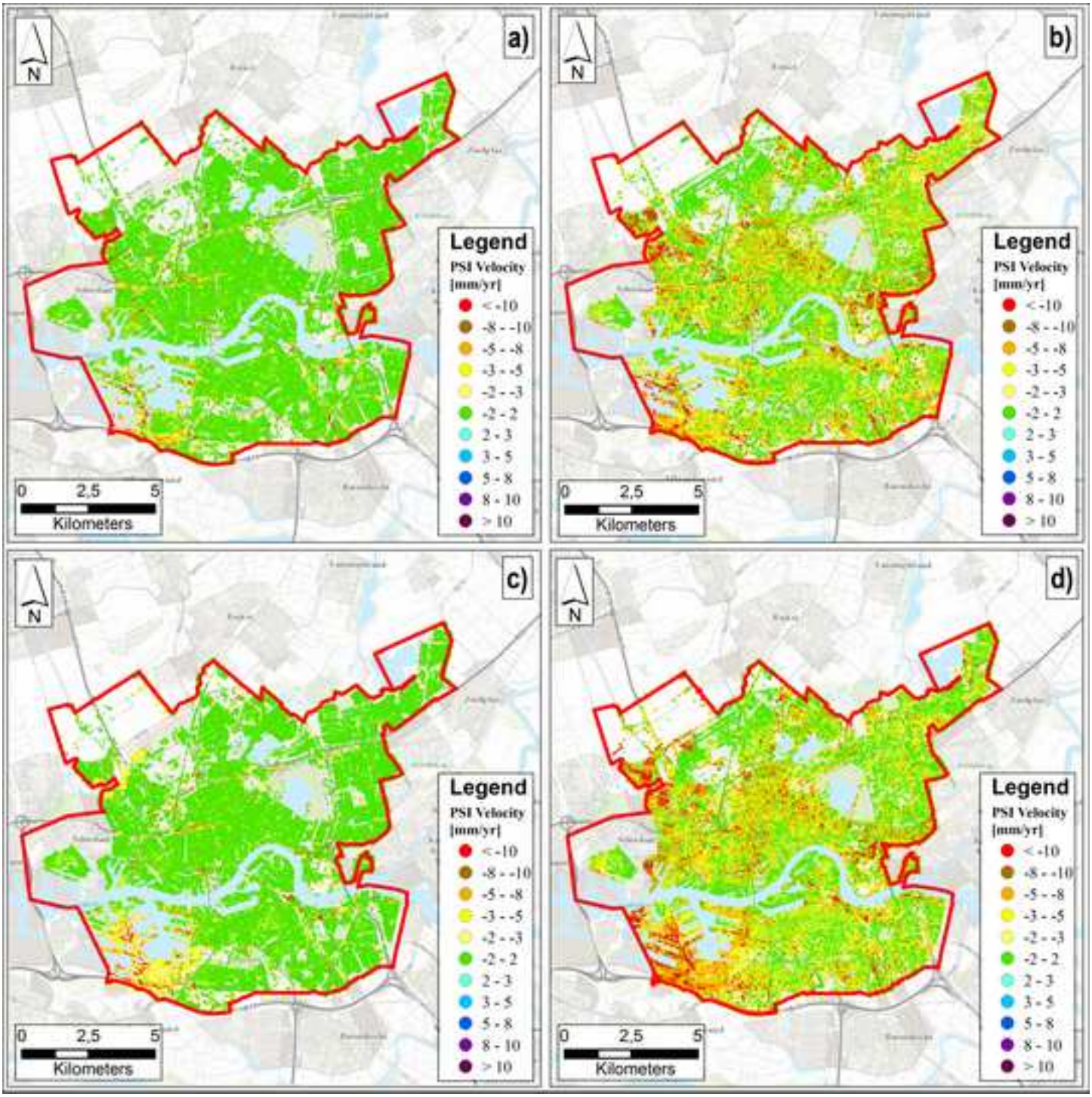

Figure_5
Click here to download high resolution image

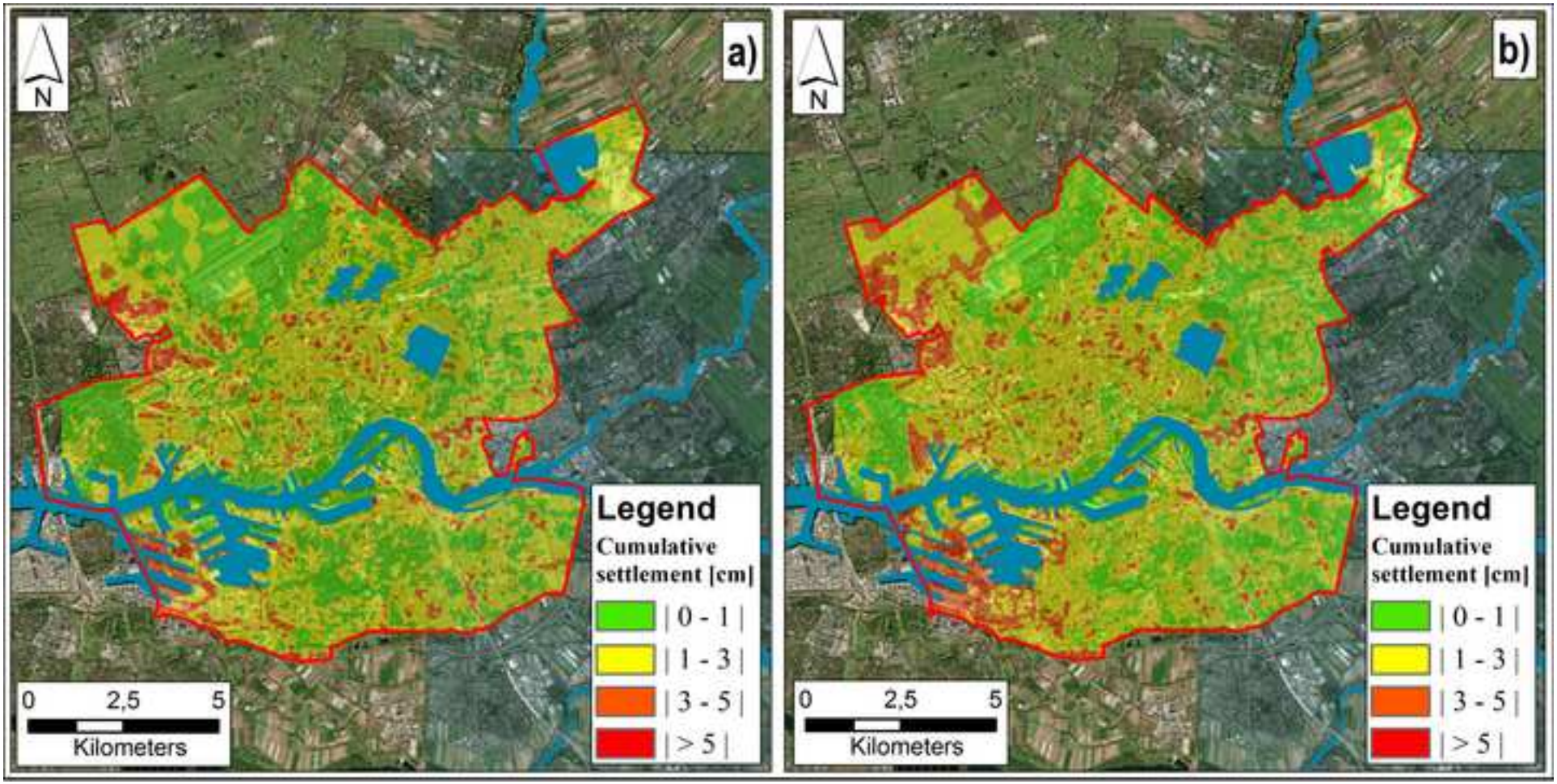

Figure_6_revised

Click here to download high resolution image

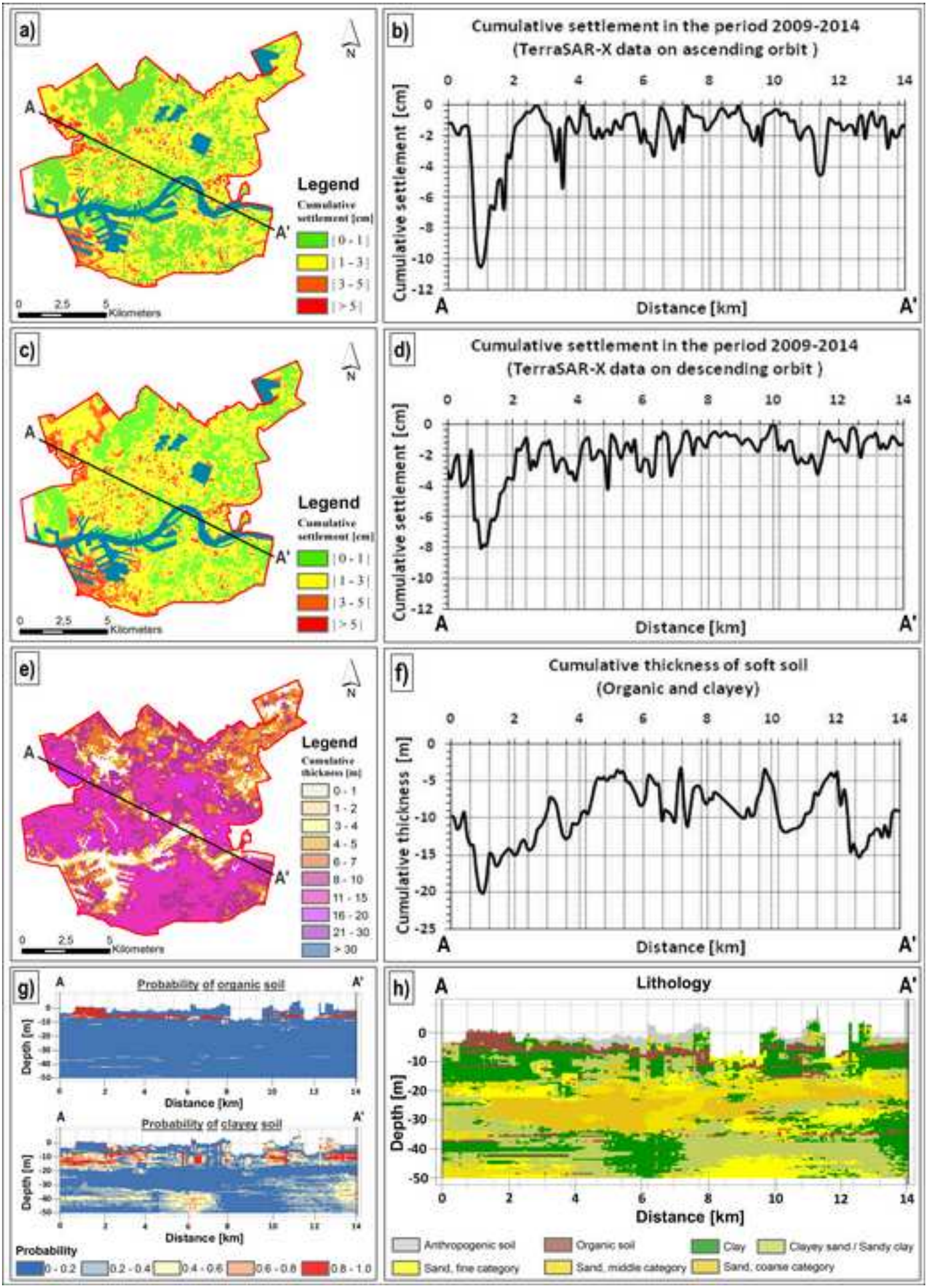

Figure_7
Click here to download high resolution image

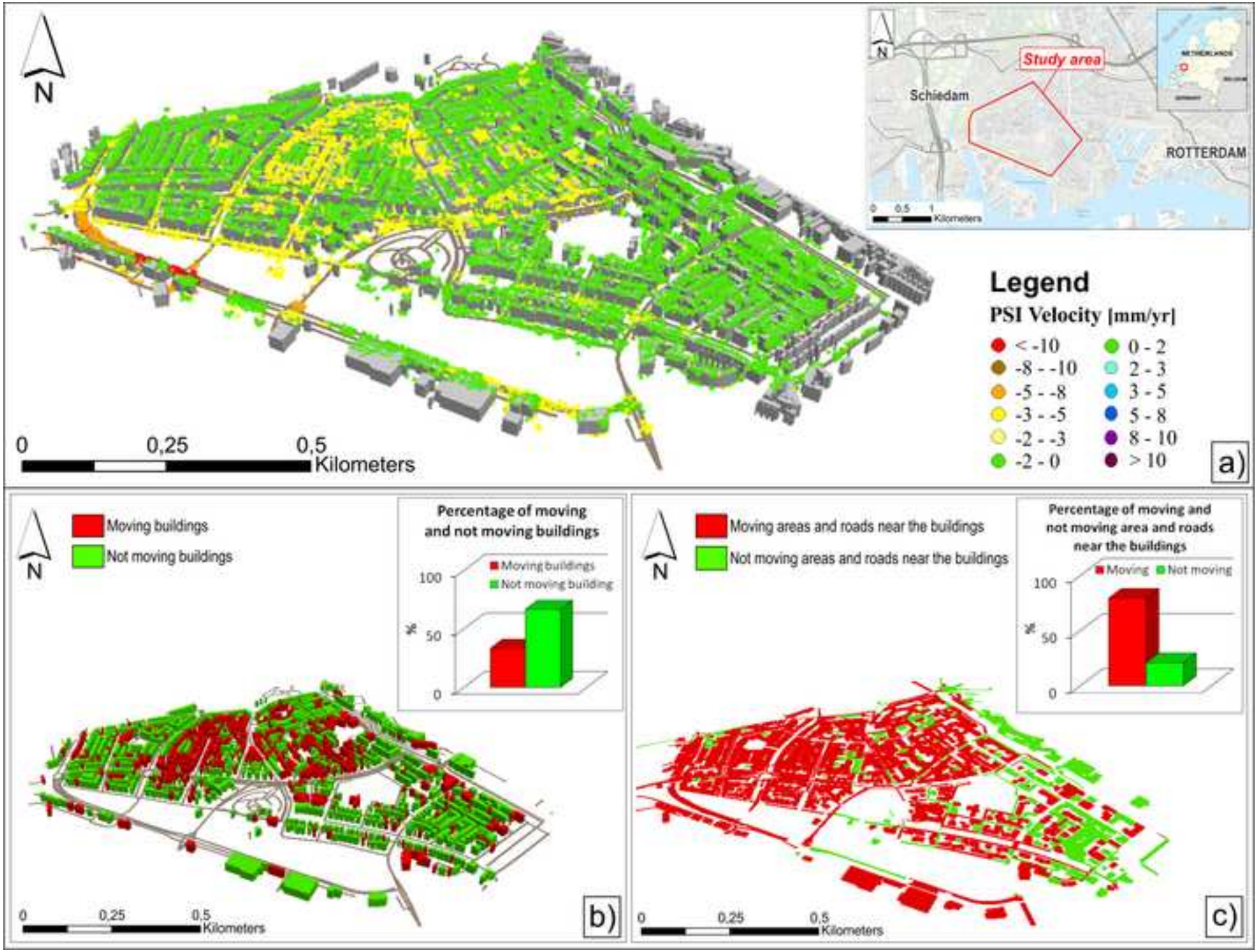

Figure_8
Click here to download high resolution image

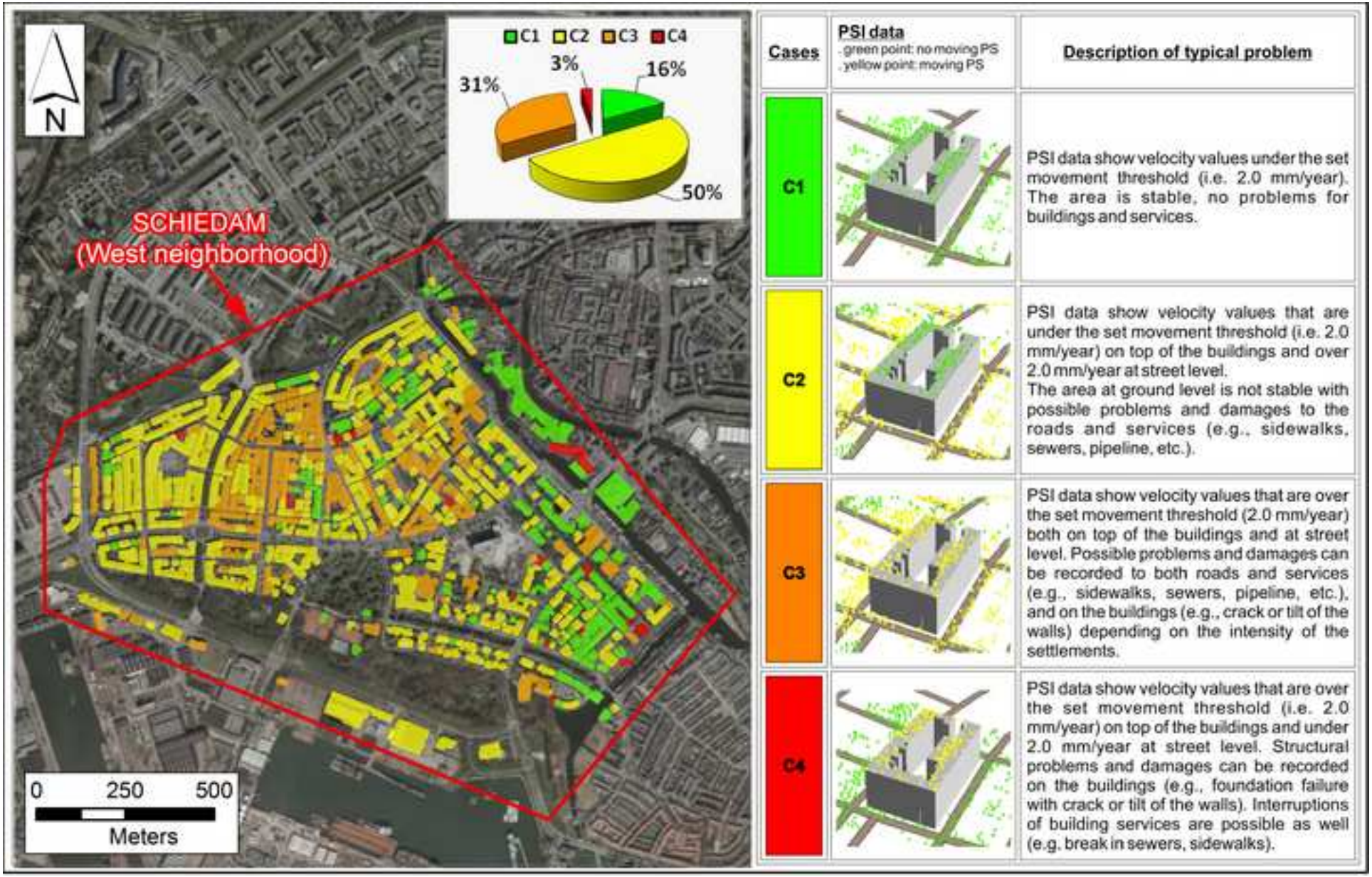

Cases	PSI data - green point: no moving PS - yellow point: moving PS	Description of typical problem
C1		PSI data show velocity values under the set movement threshold (i.e. 2.0 mm/year). The area is stable, no problems for buildings and services.
C2		PSI data show velocity values that are under the set movement threshold (i.e. 2.0 mm/year) on top of the buildings and over 2.0 mm/year at street level. The area at ground level is not stable with possible problems and damages to the roads and services (e.g., sidewalks, sewers, pipeline, etc.).
C3		PSI data show velocity values that are over the set movement threshold (2.0 mm/year) both on top of the buildings and at street level. Possible problems and damages can be recorded to both roads and services (e.g., sidewalks, sewers, pipeline, etc.), and on the buildings (e.g., crack or tilt of the walls) depending on the intensity of the settlements.
C4		PSI data show velocity values that are over the set movement threshold (i.e. 2.0 mm/year) on top of the buildings and under 2.0 mm/year at street level. Structural problems and damages can be recorded on the buildings (e.g., foundation failure with crack or tilt of the walls). Interruptions of building services are possible as well (e.g. break in sewers, sidewalks).

Figure_9
Click here to download high resolution image

BUILDING FACT-SHEETS DATE: 2015/05/12

SECTION 1: Location area and building information

Municipality	Schiedam (NL) – West neighborhood
Address	Rembrandtlaan, 12 - 36
Cordinates	51°54'44.74''N – 4°23'02.71''E
Occupancy type	Private house
Floors number	3
Construction age	1929
Structural typology	Masonry
Foundation type	Piles

SECTION 2: Background data

Geological contex

Cumulative thickness of soft soil (organic material and clay)

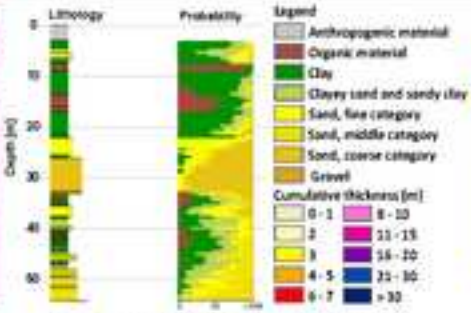

GeoTop Model – TNO Geological survey

PSI Data

TSX data (2009-2014) asc. and dsc. Orbit at street level

TSX data (2009-2014) asc. and dsc. Orbit on top of building

SECTION 3: Damage survey

Field survey photos

Classification of visible damage		
Category	Severity level	
D0	Negligible	☐
D1	Very Slight	☐
D2	Slight	☐
D3	Moderate	☐
D4	Severe	☐
D5	Very Severe	☐

Figure_10_revised

Click here to download high resolution image

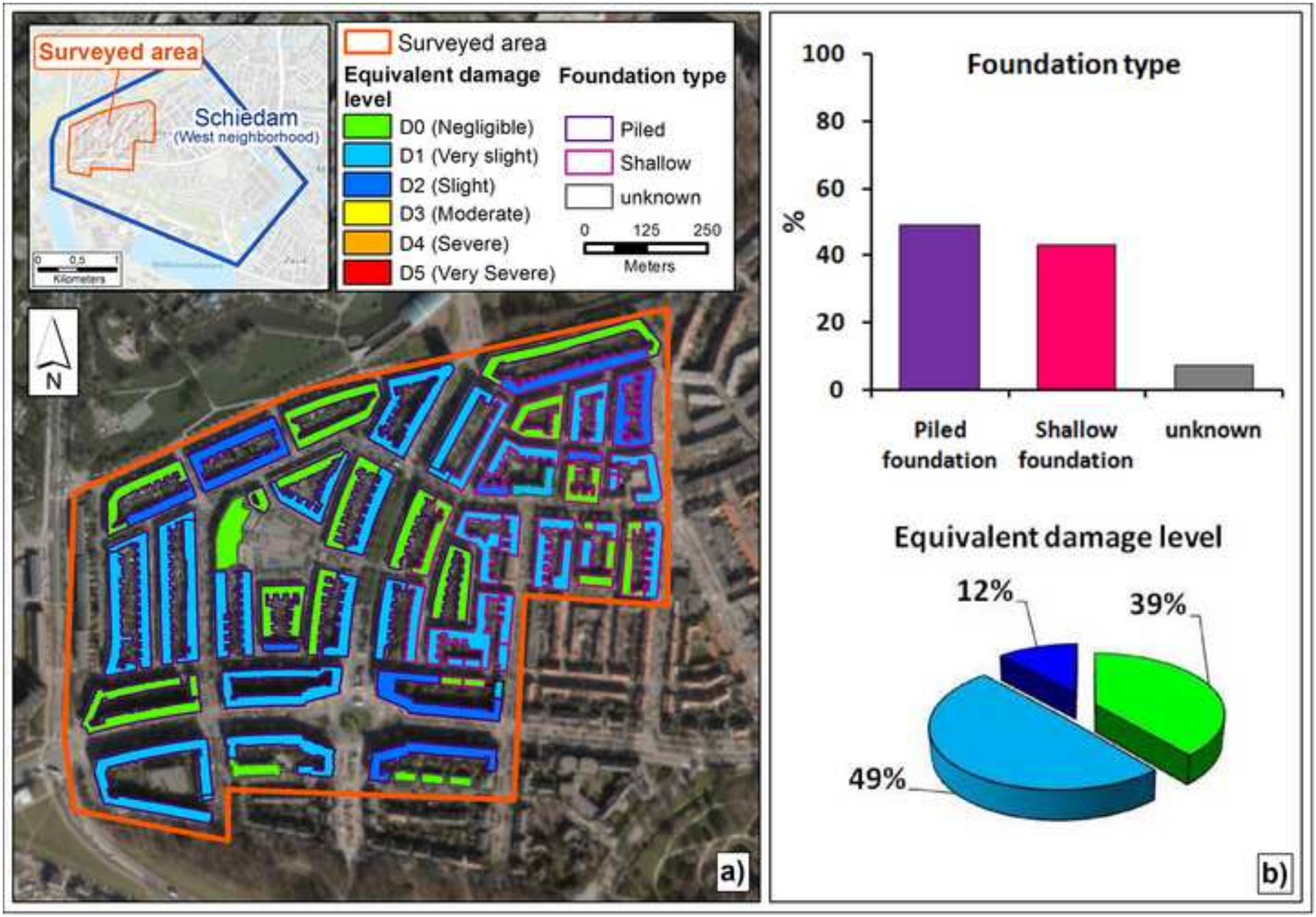

Figure_11_revised

Click here to download high resolution image

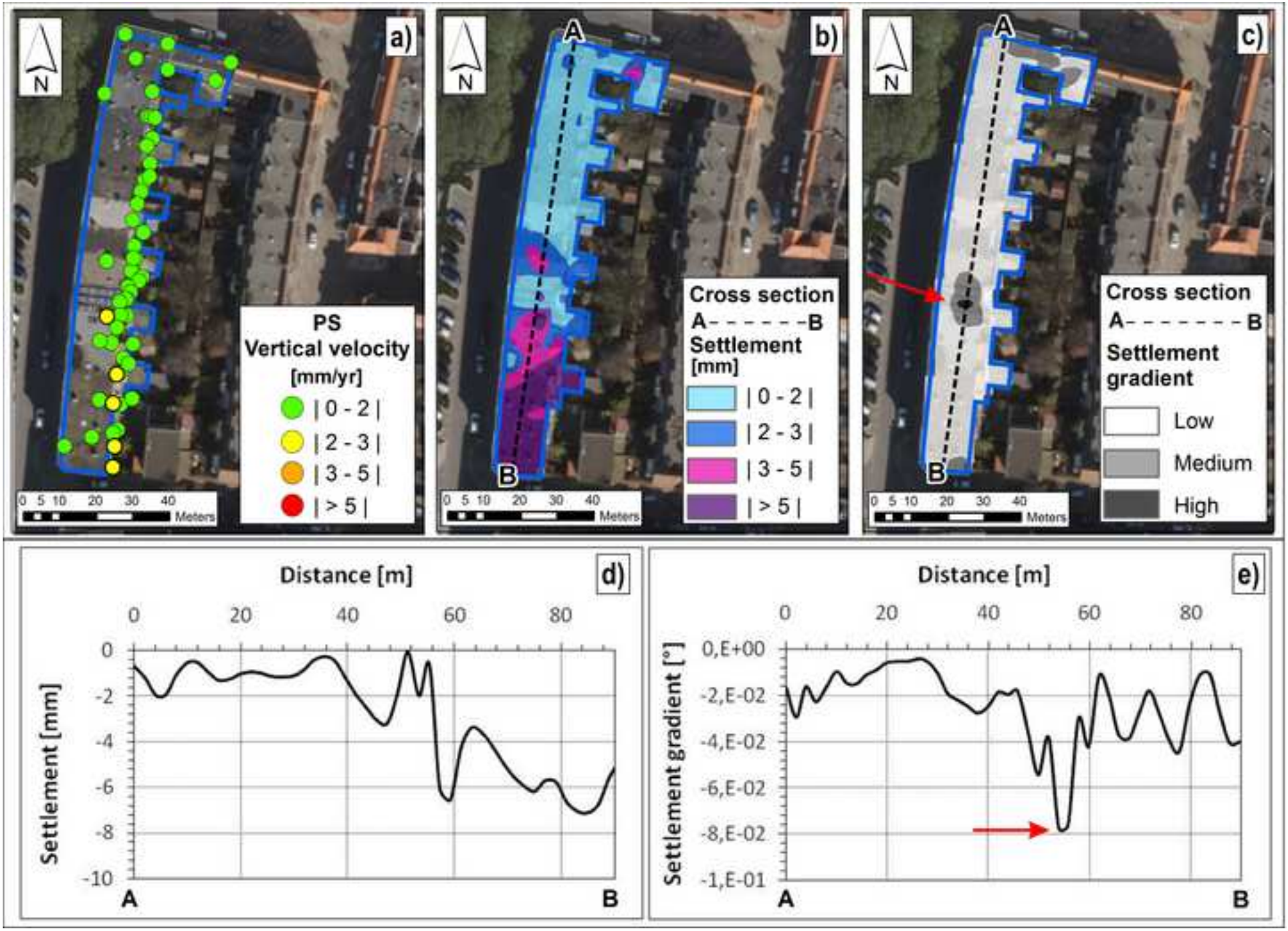

Figure_12_revised
Click here to download high resolution image

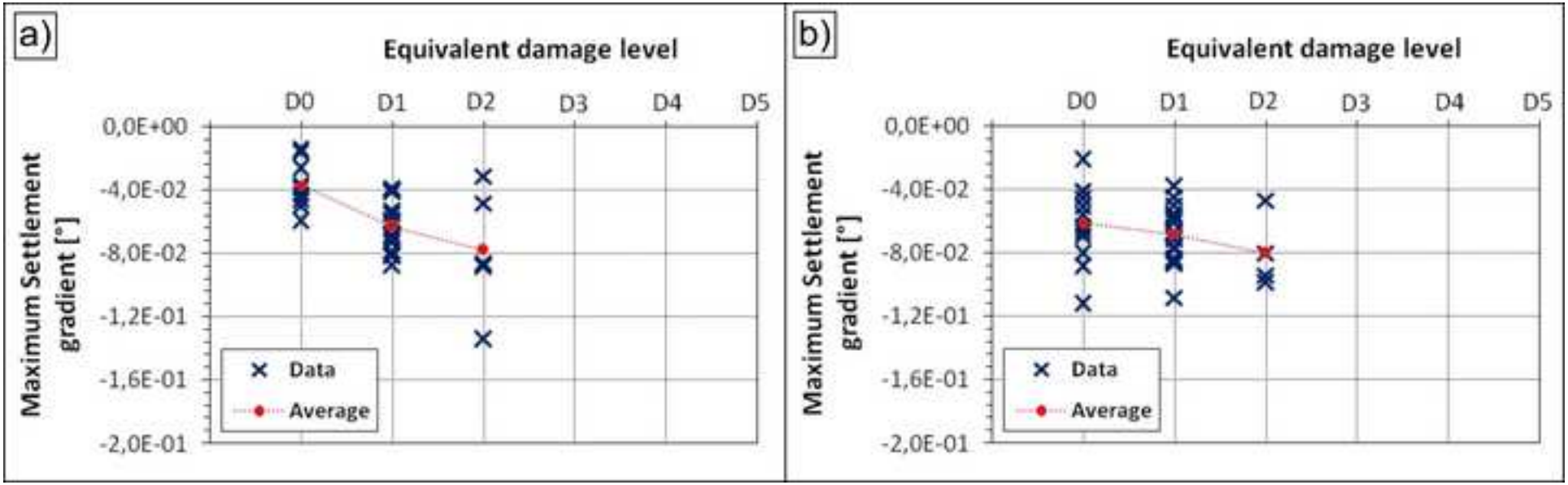

Figure_13
Click here to download high resolution image

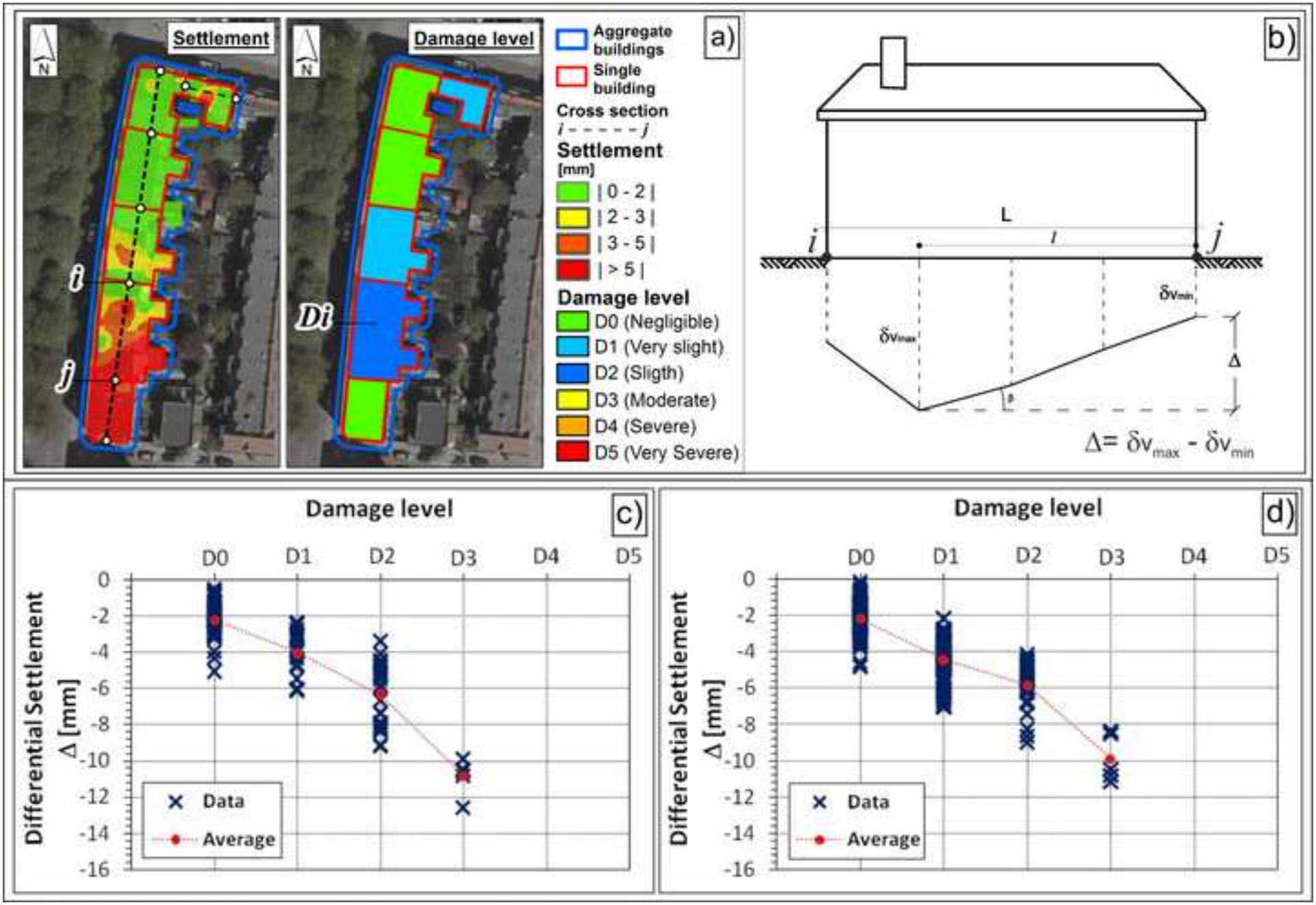

Figure_14_revised

Click here to download high resolution image

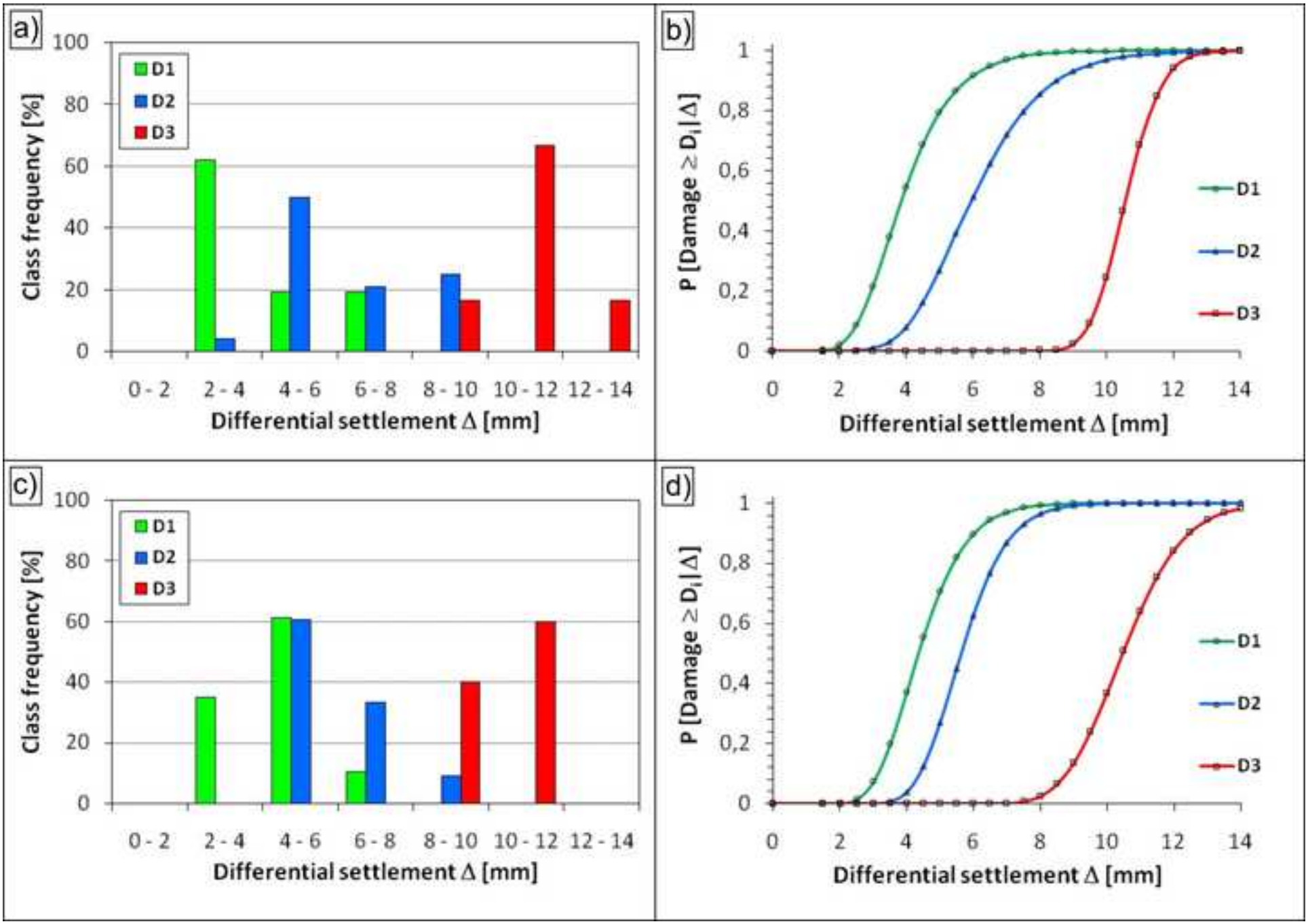

Figure_15_revised

Click here to download high resolution image